Received: 27 September 2023 | Revised: 11 December 2023 | Accepted: 27 December 2023

DOI: 10.1002/ar.25379

SPECIAL ISSUE ARTICLE

The Anatomical Record WILEY

Garzapelta muelleri gen. et sp. nov., a new aetosaur (Archosauria: Pseudosuchia) from the Late Triassic (middle Norian) middle Cooper Canyon Formation, Dockum Group, Texas, USA, and its implications on our understanding of the morphological disparity of the aetosaurian dorsal carapace

William A. Reyes[1] | **Jeffrey W. Martz**[2,3] | **Bryan J. Small**[2]

[1]Jackson School of Geosciences, The University of Texas at Austin, Austin, Texas, USA

[2]The Museum of Texas Tech University, Lubbock, Texas, USA

[3]Department of Natural Sciences, The University of Houston–Downtown, Houston, Texas, USA

Correspondence
William A. Reyes, Jackson School of Geosciences, The University of Texas at Austin, 23 San Jacinto Blvd, Austin, TX 78712, USA.
Email: will_reyes@utexas.edu

Funding information
National Science Foundation, Grant/Award Number: 2137420; Endowed Presidential Scholarship, Jackson School of Geosciences, University of Texas at Austin; Estates of Kristen Waller and Sun Youli

Abstract

The Late Triassic Dockum Group in northwestern Texas preserves a rich diversity of pseudosuchian taxa, particularly of aetosaurs. In this contribution, we present *Garzapelta muelleri* gen. et sp. nov., a new aetosaur from the Late Triassic middle Cooper Canyon Formation (latest Adamanian–earliest Revueltian teilzones) in Garza County, Texas, based on an associated specimen that preserves a significant portion of its dorsal carapace. The carapace of *G. muelleri* exhibits a striking degree of similarity between that of the paratypothoracin *Rioarribasuchus chamaensis* and desmatosuchins. We quantitatively assessed the relationships of *G. muelleri* using several iterations of the matrix. Scoring the paramedian and lateral osteoderms of *G. muelleri* independently results in conflicting topologies. Thus, it is evident that our current matrix is limited in its ability to discern the convergence within this new taxon and that our current character lists are not fully accounting for the morphological disparity of the aetosaurian carapace. Qualitative comparisons suggest that *G. muelleri* is a *Rioarribasuchus*-like paratypothoracin with lateral osteoderms that are convergent with those of desmatosuchins. Although the shape of the dorsal eminence, and the presence of a dorsal flange that is rectangular and proportionately longer than the lateral flange are desmatosuchin-like features of *G. muelleri*, the taxon does not exhibit the articulation style between the paramedian and lateral osteoderms which diagnose the Desmatosuchini (i.e., a rigid interlocking contact, and an anteromedial edge of the lateral osteoderm that overlaps the adjacent paramedian osteoderm).

KEYWORDS

Aetosaur, Dockum Group, Late Triassic, Revueltian, Texas

1 | INTRODUCTION

Aetosaurs are a Late Triassic group of quadrupedal pseudosuchian archosaurs that are characterized by their osteoderm-covered bodies, stout forelimbs, triangular skulls with laterally facing supratemporal fenestrae, partially edentulous dentaries, and body sizes ranging from 1-to-5 m in length; currently, they are documented from every continent except Australia and Antarctica (Desojo et al., 2013). In recent years, the discovery of dentigerous material for various aetosaur taxa has highlighted the disparity of the dentition among the different species (Paes-Neto et al., 2021a; Reyes et al., 2020). This has prompted researchers (e.g., Biacchi Brust et al., 2018; Desojo et al., 2013; Desojo & Ezcurra, 2011; Desojo & Vizcaíno, 2009; Paes-Neto et al., 2021a; Reyes et al., 2020; Small, 2002; von Baczko et al., 2018, 2021) to hypothesize that aetosaurs likely exhibited omnivorous/faunivorous feeding ecologies, rather than being strictly herbivorous (Walker, 1961). Most currently recognized species are documented exclusively from the Chinle Formation and Dockum Group of the southwestern United States (U.S.; Desojo et al., 2013; Parker, 2016a). In this region, aetosaur osteoderms, which are integumental ossifications independent of the main skeletal system (Scheyer et al., 2014), are some of the most commonly collected fossilized remains (Long & Ballew, 1985; Long & Murry, 1995; Parker & Martz, 2011) due to their high abundance in the aetosaurian body plan, robust nature, and ability to be easily dispersed in fluvial systems (Reyes et al., 2023; Scheyer et al., 2014).

Most aetosaur taxa (excluding *Aetosauroides scagliai*) are recovered within one of the two major clades, the Stagonolepidoidea and Aetosaurinae (Parker, 2016a, 2018b; Reyes et al., 2020, 2023). The taxa recovered within the Stagonolepidoidea (Parker, 2018b) are best exemplified by desmatosuchins such as *Desmatosuchus* (Case, 1920; Parker, 2008) and nondesmatosuchin stagonolepidoids such as *Calyptosuchus wellesi* (Case, 1932; Parker, 2018a). Taxa recovered within the Aetosaurinae (Parker, 2016a) are best exemplified by typothoracines such as *Typothorax coccinarum* (Heckert et al., 2010) and the paratypothoracin *Paratypothorax andressorum* (Long & Ballew, 1985), as well as nontypothoracines such as *Aetosaurus ferratus* (Schoch, 2007). Currently, the Aetosauria includes ~31 species (Desojo et al., 2013; Haldar et al., 2023; Parker, 2016a; Reyes et al., 2020, 2023), thus rivaling the Phytosauria as one of the most diverse and abundant archosaur groups of the Late Triassic (Ezcurra, 2016; Stocker & Butler, 2013). However, in recent years, the taxonomic status of several "dwarf" taxa (e.g., *Coahomasuchus chathamensis*, Heckert et al., 2017; *A. ferratus*, Schoch, 2007; *Polesinesuchus aurelioi*, Roberto-Da-Silva et al., 2014) has been brought to question by several researchers (Hoffman et al., 2019; Paes-Neto et al., 2021b; Paes-Neto et al., 2021c; Schoch & Desojo, 2016; Taborda et al., 2015, 2023), as they are based on skeletally immature specimens.

Due to the abundance and taxonomic variability of their osteoderms, aetosaurs are considered biostratigraphically informative as they provide an alternative means of correlating and temporally constraining Upper Triassic strata through established teilzones/holochronozones (biozones/biochronozones) which can be adapted into holochrons (biochrons; Martz & Parker, 2017; Parker & Martz, 2011). The Late Triassic estimated holochrons (sensu Martz & Parker, 2017) of western North America are biochrons derived from biostratigraphic ranges of phytosaurs (Lucas, 1998; Martz & Parker, 2017), which are large semiaquatic Late Triassic archosauriforms that superficially resemble extant crocodylians (Stocker & Butler, 2013). These holochrons in order from oldest to youngest are the Otischalkian, Adamanian, Revueltian, and Apachean (Lucas, 1998; Martz & Parker, 2017). The Dockum Group contains all four holochronozones on which the holochrons are based (Martz & Parker, 2017). Currently, stagonolepidoids (including the desmatosuchins) are known only from the Otischalkian and Adamanian holochronozones, while typothoracine and paratypothoracin aetosaurs characterize Revueltian and Apachean holochronozones (Long & Ballew, 1985; Long & Murry, 1995; Martz & Parker, 2017; Parker & Martz, 2011); however, typothoracines and stagonolepidoids do co-occur within the late Adamanian holochron (Martz et al., 2013; Parker & Martz, 2011). It is hypothesized that the extinction of stagonolepidoid taxa in the southwestern U.S. occurred at the Adamanian–Revueltian boundary (~215 Ma; Dunlavey et al., 2009; Parker & Martz, 2011; Ramezani et al., 2011, 2014; Rasmussen et al., 2020).

In addition to their biostratigraphic significance, the morphology of aetosaur dorsal osteoderms plays a fundamental role in our understanding of evolutionary relationships within the Aetosauria (Parker, 2016a). Most aetosaurs can be placed within three broad body shapes: narrow-bodied and lacking prominent spines on the lateral osteoderms, narrow bodied with prominent spines on the lateral osteoderms, and broad-bodied with wide paramedian osteoderms (Desojo et al., 2013; Parker, 2016a). Historically, these body forms were thought to represent three monophyletic groups (Parker, 2007); however, narrow-bodied forms are now recognized as a paraphyletic group of basal aetosaurs that include the early-diverging members of the spinose and wide-bodied clades (Desojo et al., 2012, 2013; Parker, 2016a). The Stagonolepidoidea (Parker, 2018a, 2018b; Reyes et al., 2020) includes the spinose desmatosuchins (e.g., *Desmatosuchus spurensis*, Case, 1920; Parker, 2008), and the narrow-bodied,

nonspinose, nondesmatosuchins (e.g., *C. wellesi*, Case, 1932; Long & Ballew, 1985). On the other hand, the Aetosaurinae includes the wide-bodied typothoracines (e.g., *T. coccinarum*, Cope, 1875; Heckert et al., 2010; Long & Ballew, 1985), and the narrow-bodied, nonspinous, nontypothoracines (e.g., *Coahomasuchus kahleorum*, Heckert & Lucas, 1999). Additionally, many aetosaur taxa can sometimes be identified based solely on a combination of osteoderm characters including dorsal ornamentation, proportional shape, and the presence or absence of spines or horns (Desojo et al., 2013; Parker, 2016a; Reyes et al., 2023). Several taxa are known solely or primarily from isolated osteoderms including *Lucasuchus hunti* (Long & Murry, 1995), *Rioarribasuchus chamaensis* (Parker, 2007; Zeigler et al., 2003), *Tecovasuchus chatterjeei* (Martz & Small, 2006), *Apachesuchus heckerti* (Spielman & Lucas, 2012), *Adamanasuchus eisenhardtae* (Lucas et al., 2007), *Sierritasuchus macalpini* (Parker et al., 2008), *Redondasuchus rineharti* (Spielmann et al., 2006), *Kocurypelta sylvestris* (Czepiński et al., 2021), *Venkatasuchus armatum* (Haldar et al., 2023), and *Kryphioparma caerula* (Reyes et al., 2023).

In 1989, paleontologist Bill Mueller and local amateur collector Emmett Shedd discovered several fossilized remains in MOTT 3882 (the UU Sand Creek locality) within the middle unit of the Cooper Canyon Formation (Martz, 2008), which spans the Adamanian-Revueltian boundary (Figure 1; Martz, 2008). The most notable fossilized remains were the abundant paramedian and lateral osteoderms and ribs of a large, associated aetosaur skeleton (TTU-P 10449). Preliminary studies by Martz et al. (2003) suggested that TTU-P 10449 likely represented a new taxon, because of its morphological similarities to both *R. chamaensis* and *Desmatosuchus* (Martz, 2008). In this contribution we formally describe TTU-P 10449 and designate this specimen as the holotype of *Garzapelta muelleri* gen. et sp. nov., a new aetosaur that is predominantly based on associated osteoderms. Additionally, we

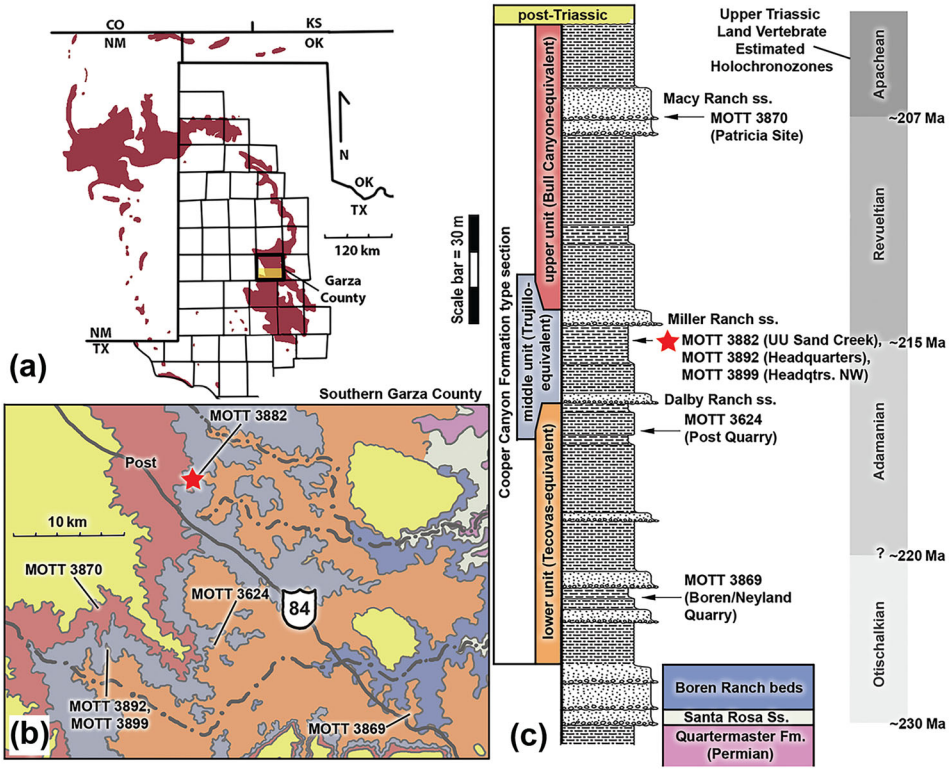

FIGURE 1 Location of MOTT 3882 (the UU Sand Creek locality; labeled with a red star) and that of other biostratigraphically relevant localities within the Cooper Canyon Formation in southwestern Garza County, Texas, USA. (a) Geographic exposures of the Dockum Group (shaded in red) in the southwestern U.S. (b) enlarged geologic map of highlighted area in (a) shows simplified geologic map of the Dockum Group in southern Garza County (see stratigraphic section for explanation of unit colors) showing approximate location of important vertebrate localities, data from Martz (2008). (c) Stratigraphic range of Upper Triassic Land Vertebrate Estimated Holochronozones are based on Martz and Parker (2017), with numeric ages derived from Atchley et al. (2013), Dunlavey et al. (2009), Ramezani et al. (2011, 2014), and Rasmussen et al. (2020); the latter two references provide revised age constraints for the base of the Adamanian and Otischalkian from those of Martz and Parker (2017). CO, Colorado; Fm., Formation. Ka, Kansas; Ma, Million years; MOTT, Museum of Texas Tech; NM, New Mexico; OK, Oklahoma; ss., sandstone; TX, Texas.

qualitatively and quantitatively explore the phylogenetic relationships of *G. muelleri* within the Aetosauria.

2 | GEOLOGICAL SETTING

In the western U.S., Upper Triassic continental strata extend across the southwest and into the Rocky Mountains (Lehman & Chatterjee, 2005; Lucas, 1993; Martz et al., 2017). The Dockum Group (Figure 1) extends from western Texas through eastern New Mexico and adjacent regions of Oklahoma and Colorado (Lehman & Chatterjee, 2005), while the Chinle Formation occurs primarily in the Colorado Plateau region of New Mexico, Utah, Colorado, and Arizona (Lucas, 1993; Martz et al., 2012, 2017). The Chugwater Group occurs in northern Colorado and Utah, Wyoming, and parts of Idaho and Montana (Fitch et al., 2023; Lovelace et al., 2023). Historically, there has been disagreement regarding Upper Triassic stratigraphic nomenclature in the southwestern U.S. because Lucas (1993) proposed abandoning the term "Dockum Group" and elevating the Chinle Formation to group status to encompass all Upper Triassic continental strata in the western United States; this proposal by Lucas (1993) was based on the argument that the historical usage of the term "Dockum Group" was confusing and inconsistent. The proposal has not been broadly adopted and we maintain the Dockum Group and Chinle Formation as two separate stratigraphical units following other workers (e.g., Hungerbühler et al., 2013; Lehman & Chatterjee, 2005; Lessner et al., 2018; Martz et al., 2013; Sarigül, 2016, 2017, 2018).

The Dockum Group was deposited primarily by braided and meandering river systems originating from the Ouachita-Marathon Orogenic Belt to the South and Amarillo-Wichita Uplift to the North, with some strata dominated by lacustrine deposits (Lehman & Chatterjee, 2005; Walker & Holbrook, 2023). In northeastern New Mexico and the Texas Panhandle the stratigraphy of the Dockum Group is composed of five or six formations; from oldest to youngest they are the Santa Rosa and/or Camp Springs, Tecovas and/or Garita Creek, Trujillo, Bull Canyon, and Redonda formations (Lehman & Chatterjee, 2005; Lucas, 1993; Martz & Parker, 2017). The southern Texas exposures in Garza County and Borden County are grouped into the Cooper Canyon Formation (Lehman et al., 1992; Lehman & Chatterjee, 2005), which is subdivided into lower, middle, and upper sections that are considered stratigraphically equivalent to the Tecovas, Trujillo, and Bull Canyon formations, respectively (Figure 1; Martz, 2008; Martz et al., 2013).

The holotype specimen of *G. muelleri* (TTU-P 10449) was collected from MOTT 3882 (the UU Sand Creek locality) in southern Garza County, which is stratigraphically located a few meters below the Miller Ranch Sandstone (Figure 1; Martz, 2008, p. 245) in the Trujillo-equivalent middle Cooper Canyon Formation (Figure 1). The fossil-bearing horizon at MOTT 3882 is characterized as a 10 cm thick medium-coarse grained sandstone (Martz, 2008, p. 245). The fossil assemblage includes the type specimen of *G. muelleri* gen. et sp. nov. (TTU-P 10449, this study), the type specimen of the procolophonid *Libognathus sheddi* (DMNH V.20491, Mueller et al., 2023; Small, 1997), and an isolated archosauromorph vertebra referred to cf. "*Procoelosaurus*" (Atannasov, 2002).

The Miller Ranch sandstone is stratigraphically located several meters above the lowest known stratigraphic occurrence (LO_K) of the phytosaur *Machaeroprosopus* from MOTT 3892 (the Headquarters locality; Martz, 2008), which defines the base of the Revueltian holochronozone (sensu Martz & Parker, 2017) within the Cooper Canyon Formation (Figure 1; Hungerbühler et al., 2013; Lessner et al., 2018; Martz, 2008; Martz et al., 2013; Sarigül, 2016, 2017, 2018). However, the precise position of MOTT 3882 (UU Sand Creek locality) relative to the LO_k of *Machaeroprosopus* is uncertain, making it unclear if the locality is latest Adamanian or earliest Revueltian although the latter interpretation is favored (Martz, 2008, p. 245). Radiometric dates from the Chinle Formation of Petrified Forest National Park place the transition between the Adamanian and Revueltian holochrons somewhere between 214 and 217.5 Ma in the middle Norian (Atchley et al., 2013; Martz & Parker, 2017; Rasmussen et al., 2020), making this the best broad approximation for the age of MOTT 3882.

3 | METHODS

3.1 | Collections and preparation

Collection and preparation records associated with TTU-P 10449 are limited. The records only include information on the type locality MOTT 3882, limited field photographs associated with the locality and excavation of TTU-P 10449, and a 1 ft^2 grid map showing the association of the individual elements (Figure 2); however, the individual elements of TTU-P 10449 are not properly labeled on the grid map, which limits our ability to use their association in the field as a proxy in our anatomical interpretations. Nonetheless, it does indicate that a significant portion of the skeleton was preserved in one cluster. The elements of TTU-P 10449 were excavated using a combination of brushes, sharp pointed tools, water, and dissolvable glue. They were collected primarily as

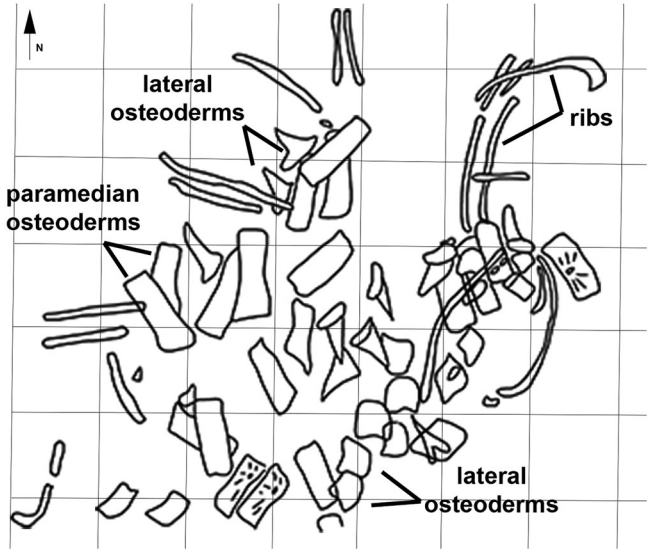

FIGURE 2 A 1 ft^2 grid map showing part of the associated skeleton of *Garzapelta muelleri* gen. et sp. nov. (TTU-P 10449) within MOTT 3882 (the UU Sand Creek Locality). Outlines of ribs, paramedian and lateral osteoderms are labeled accordingly. N, North.

fragments into individual zip-lock bags. The elements were primarily cleaned with water and pin-vices to remove the excess matrix, and later reconstructed using the reversible glue Butvar-72. The elements of TTU-P 10449 were photographed using a Nikon D3500 DSR with a 20–70 mm wide-angle lens.

3.2 | Phylogenetic methods

Garzapelta muelleri gen. et sp. nov. was incorporated and scored into the most recent matrix of the Aetosauria by Haldar et al. (2023), which expands on those of Paes-Neto et al., (2021b), Parker (2016a), and Reyes et al. (2020), using Mesquite v.3.81 (Maddison & Maddison, 2023). We a priori omitted *Aetobarbakinoides brasiliensis* because it was considered a wildcard taxon by previous authors (e.g., Heckert et al., 2015; Parker, 2016a). Additionally, we excluded *P. aurelioi* (Roberto-Da-Silva et al., 2014) from our analysis following the discussion by Paes-Neto et al., (2021c) suggesting that *P. aurelioi* is a junior synonym of *A. scagliai*. Unfortunately, *K. caerula* (Reyes et al., 2023) remains too fragmentary to quantitatively assess its phylogenetic relationships. Also, we modified the scorings of several taxa based on recently published literature, photographs, and personal observation of specimens (see Supporting information S1 and S2). Thus, the new matrix includes 29 taxa (two outgroups) and 104 characters (47 cranial, 57 postcranial), where characters 52, 53, 65, 81, 97, and 98 were modified in this study (see Supporting information S1 and S2). The dataset was analyzed using both parsimony and Bayesian inference to explore alternative phylogenetic hypotheses of the Aetosauria. We assessed the topological position of *G. muelleri* by running three different versions of the matrix for both parsimony and Bayesian inference (a total of six analyses) with the goal of independently assessing the phylogenetic signal of the recovered paramedian and lateral osteoderms of TTU-P 10449. These iterations of the matrix are (1) only paramedian osteoderms scored for *G. muelleri*, (2) only lateral osteoderms scored for *G. muelleri*, and (3) all osteoderms scored for *G. muelleri*; additionally, we ran a fourth iteration where we omitted *G. muelleri* to provide a comparison aspect in our assessment of the influence *G. muelleri* has on the topology of the Aetosauria. The characters were omitted from iterations one and two in accordance if they were specific to the morphology of the respective osteoderm (e.g., asymmetry of the lateral osteoderm, width to length ratio of a paramedian osteoderm). However, characters that can be inferred based on the presence of an isolated paramedian or lateral osteoderm were scored (e.g., the morphology of the lateral margin of a paramedian osteoderm can be inferred based on the morphology of the medial edge of the adjacent lateral osteoderm when the paramedian osteoderm is not preserved). The character list and associated matrices can be found in both TNT and Nexus versions with the associated text file in the Supporting information S1 and S2.

Maximum parsimony was employed using the phylogenetic analysis software package TNT v1.5 (Goloboff et al., 2008) using the traditional search option with 1000 replications and tree bisection reconnection swapping while keeping 10 trees per replication and condensing zero-length branches. Fourteen characters (3, 4, 14, 20, 22, 23, 24, 28, 64, 70, 73, 76, 79, and 83) were ordered following analyses by Paes-Neto et al., (2021b), Parker (2016a), and Reyes et al. (2020). The parsimony analysis of iteration one (i.e., only paramedian osteoderms) resulted in seven most-parsimonious trees (MPTs) with a length of 280 steps, a Consistency Index of 0.532, and a Retention Index of 0.687; iteration two (i.e., only lateral osteoderms) resulted in 29 MPTs with a length of 277 steps, a Consistency Index of 0.534, and a Retention Index of 0.691; iteration three (i.e., all osteoderms) resulted in 29 MPTs with a length of 284 steps, a Consistency Index of 0.528, and a Retention Index of 0.685; and iteration four (*G. muelleri* omitted) resulted in 7 MPTs with a length of 271 steps, a Consistency index of 0.554, and a Retention index of 0.716. The strict consensus of the MPTs are each discussed below. The Bayesian inference analysis was performed using the phylogenetic analysis software MrBayes v3.2.6 (Huelsenbeck & Ronquist, 2001) with the Mkv model

and gamma rate variation under the following parameters: two runs with four Markov chain Monte Carlo chains each, sampled every 1000 generations, for 5 million generations with a relative burn-in frequency of 0.25. Convergence of independent runs was assessed using Tracer v.1.7.1 (http://beast.bio.ed.ac.uk/Tracer). For consistency, we ordered the same 14 characters listed above. The consensus cladogram.

3.3 | Institutional abbreviations

CPE2, Coleção Municipal, São Pedro do Sul, Brazil; DMNH, Perot Museum of Nature and Science (formerly the Dallas Museum of Natural History), Dallas, Texas, USA; DMNH V, Denver Museum of Nature and Science, Denver, Colorado, USA; MCN, Museu de Ciências Naturais, Secretaria Estadual do Meio Ambiente e Infraestrutura, Porto Alegre, Brazil; MCP, Museu de Ciências e Tecnologia dae Pontifícia Universidade Católica do Rio Grande do Sul, Porto Alegre, Brazil; MCZ, Museum of Comparative Zoology, Cambridge, Massachusetts, USA; MOTT, refers to locality from TTU-P; MNA, Museum of Northern Arizona, Flagstaff, Arizona, USA; NCSM, North Carolina Museum of Natural Sciences, Raleigh, North Carolina, USA; NHMUK, Natural History Museum, London, England, UK; NMMNH, New Mexico Museum of Natural History and Science, Albuquerque, New Mexico, USA; PEFO, Petrified Forest National Park, Arizona, USA; PFV, refers to a locality number from PEFO; PVL, Instituto Miguel Lillo, Paleontología de Vertebrados, Tucumán, Argentina; SMNS, Staatliches Museum für Naturkunde, Stuttgart, Germany; TMM, Texas Vertebrate Paleontology Collections, Austin, Texas, USA; TTU-P, Museum of Texas Tech University, Lubbock, Texas, USA; UCMP, University of California Museum of Paleontology, Berkeley, California, USA; ULBRA PVT, Universidade Luterana do Brasil, Coleção de Paleovertebrados, Canoas, Rio Grande do Sul, Brazil; UFSM, Laboratório de Estratigrafia e Paleobiologia of Universidade Federal de Santa Maria, Santa Maria, Rio Grande do Sul, Brazil; UMMP, University of Michigan Museum of Paleontology, Ann Arbor, Michigan, United States; ZPAL, Institute of Paleobiology, Polish Academy of Sciences, Warsaw, Poland.

4 | SYSTEMATIC PALEONTOLOGY

Archosauria Cope, 1869, sensu Gauthier & Padian, 1985.

Pseudosuchia Zittel, 1887–1890, sensu Gauthier & Padian, 1985.

Aetosauria Marsh, 1884, sensu Parker, 2007.

Stagonolepididae Lydekker, 1887, sensu Heckert & Lucas, 2000.

Stagonolepidoidea Parker, 2018b.

Garzapelta gen. nov.

G. muelleri gen. et sp. nov.

4.1 | Etymology

The genus name *Garza* honors Garza County in Texas, where the type specimen was discovered +Latin *pelta* shield, alluding to the carapace that characterizes aetosaurs. The species name *muelleri* is in honor and memory of Bill D. Mueller for his many contributions to Texas Triassic paleontology and his early work on this aetosaur project.

4.2 | Diagnosis

Garzapelta muelleri gen. et sp. nov. is a large-bodied aetosaur with autapomorphic conditions that include protuberances on the anteriorly keeled dorsal eminence (i.e., spine) of the lateral osteoderms in the cervical and anterior-trunk region, a strongly sigmoidal contact between the paramedian and lateral osteoderms of the anterior-caudal region, a sinuous posterior margin of the anterior caudal paramedian osteoderms that exhibits a posteriorly projecting "tongue"-like process directly posterior to the dorsal eminence, an anterior margin in precaudal dorsal osteoderms that is a thin, smooth, unornamented strip of bone, and variation in the development of an anterior bar between the precaudal and caudal regions. *Garzapelta muelleri* is also differentiated from other aetosaurs based on a unique combination of morphological characters. These include lateral osteoderms with well-developed, moderately long, recurved spines (shared with *Longosuchus meadei*, *L. hunti*, and *S. macalpini*), a dorsal eminence that lacks a posterior embayment near its base on the lateral osteoderms (as observed in *L. hunti* and *Desmatosuchus*), mid-trunk lateral osteoderms that are strongly asymmetrical and exhibit an obtuse flexure between the reduced lateral flange and much larger dorsal flange (unlike those of typothoracines and desmatosuchins, but similar to most other aetosaurs), a semicircular lateral flange in anterior caudal lateral osteoderms (shared with paratypothoracins), a distinct medially projecting convex process on the anteromedial edge of the lateral osteoderm (shared with *R. chamaensis*), paramedian and lateral osteoderms

that lack a strong ridge-and-groove articulation between them (unlike desmatosuchins), trunk paramedian osteoderms with a dorsal eminence that is medially offset and does not contact the posterior margin (similar to paratypothoracins), mid-trunk paramedian osteoderms that exhibit a maximum width-to-length ratio (W:L) between 3.0 and 3.5 (smaller than those of typothoracines except *R. chamaensis*), paramedian osteoderms with a dorsal ornamentation composed of grooves and ridges that radiate from the dorsal eminence (shared with most taxa except desmatosuchins, *T. coccinarum*, and *R. rineharti*), paramedian osteoderms that overlap the anteromedial edge of the lateral osteoderm (unlike desmatosuchins), and paramedian osteoderms with a short rounded anterolateral process (shared with *A. scagliai*, *A. ferratus*, and typothroracines).

4.3 | Holotype

TTU-P 10449, an associated skeleton preserving several paramedian and lateral osteoderms from the cervical to caudal regions, trunk ribs, and a fragmentary podial.

4.4 | Type locality and age

The type specimen of *G. muelleri* gen. et sp. nov. (TTU-P 10449) was collected from MOTT 3882 (the UU Sand Creek Locality) within the middle Cooper Canyon Formation (=Trujillo Formation), Dockum Group, in Garza County, Texas (Figure 1; Martz, 2008). Current litho- and biostratigraphic constraints of the Dockum Group indicate that *G. muelleri* is middle Norian in age and lies within either the latest Adamanian holochon or earliest Revueltian holochron (Figure 1; Martz et al., 2013; Martz & Parker, 2017).

5 | OSTEOLOGICAL DESCRIPTION

5.1 | Paramedian osteoderms

TTU-P 10449 was recovered with an associated carapace that includes elements from both the left and right sides of the body (Figure 2). Overall, the osteoderms are moderately to well preserved, with most exhibiting poorly preserved anterior edges. A large portion of the disarticulated carapace of TTU-P 10449 is preserved in close association (Figure 2) and includes a total of 38 paramedian osteoderms and 34 lateral osteoderms. No ventral or appendicular osteoderms are preserved in TTU-P 10449. Although the quarry map (Figure 2) does not assist strongly in placing the osteoderms in an anterior-to-posterior sequence, several lateral and paramedian osteoderms in TTU-P 10449 can be articulated, allowing them to be paired. Moreover, several aetosaur taxa preserve extensive portions of their carapace (see Supporting information S1 and S2; Desojo et al., 2013; Long & Murry, 1995), with some being fully articulated, thus allowing us to assess the relative position of the preserved osteoderms in TTU-P 10449.

Based on this it is evident that the aetosaurian carapace (Figure 3) is composed of four anteroposterior columns and several transverse rows that include two pairs of paramedian and lateral osteoderms. Additionally, the dorsal carapace can be divided (Figure 3) into several regions (i.e., cervical, trunk, sacral, caudal) and subregions (i.e., anterior-, mid-, posterior-) with general trends in morphology across its various regions. Paramedian osteoderms that are crescentic in dorsal view occur in the cervical and anterior-trunk regions (Martz, 2002; Parker, 2016b). Dorsal ornamentation becomes pronounced/incised posteriorly along the dorsal carapace, being faintest in the cervical region and most developed in the pelvic and anterior-caudal regions before becoming faint again more posteriorly in the tail (Parker, 2007). The dorsal ornamentation pattern remains fairly uniform across the carapace only varying in degree of incision (variation in dorsal ornamentation has only been documented in one individual of *A. scagliai*, PVL 2073 (Taborda et al., 2015, figure 4). If present, the dorsal eminence becomes more pronounced and centralized posteriorly along the dorsal carapace into the anterior-caudal region before becoming reduced more posteriorly (Parker, 2007). Paramedian osteoderms are transversely widest in the trunk region, often are transversely flexed at the center of ossification in the posterior-most portion of the anterior-caudal region, and gradually become longer than wide into the posterior caudal region.

The described criteria allow us to hypothesize the regions (Figure 3) from which the preserved osteoderms are derived in the carapace of TTU-P 10449 and describe them in a relative anterior to posterior sequence. It is evident that TTU-P 10449 preserves osteoderms derived from the cervical through caudal regions; however, no ventral or appendicular osteoderms are preserved. (Figure 3). The following description and figures focus primarily on paramedian and lateral osteoderms that pair with each other, and elements that best exemplify the morphology of *G. muelleri* gen. et sp. nov.

5.1.1 | Cervical and anterior trunk regions

The cervical paramedian osteoderms (Figure 4) are proportionately small, similar to those from the caudal region; however, they lack the transverse ventral arching

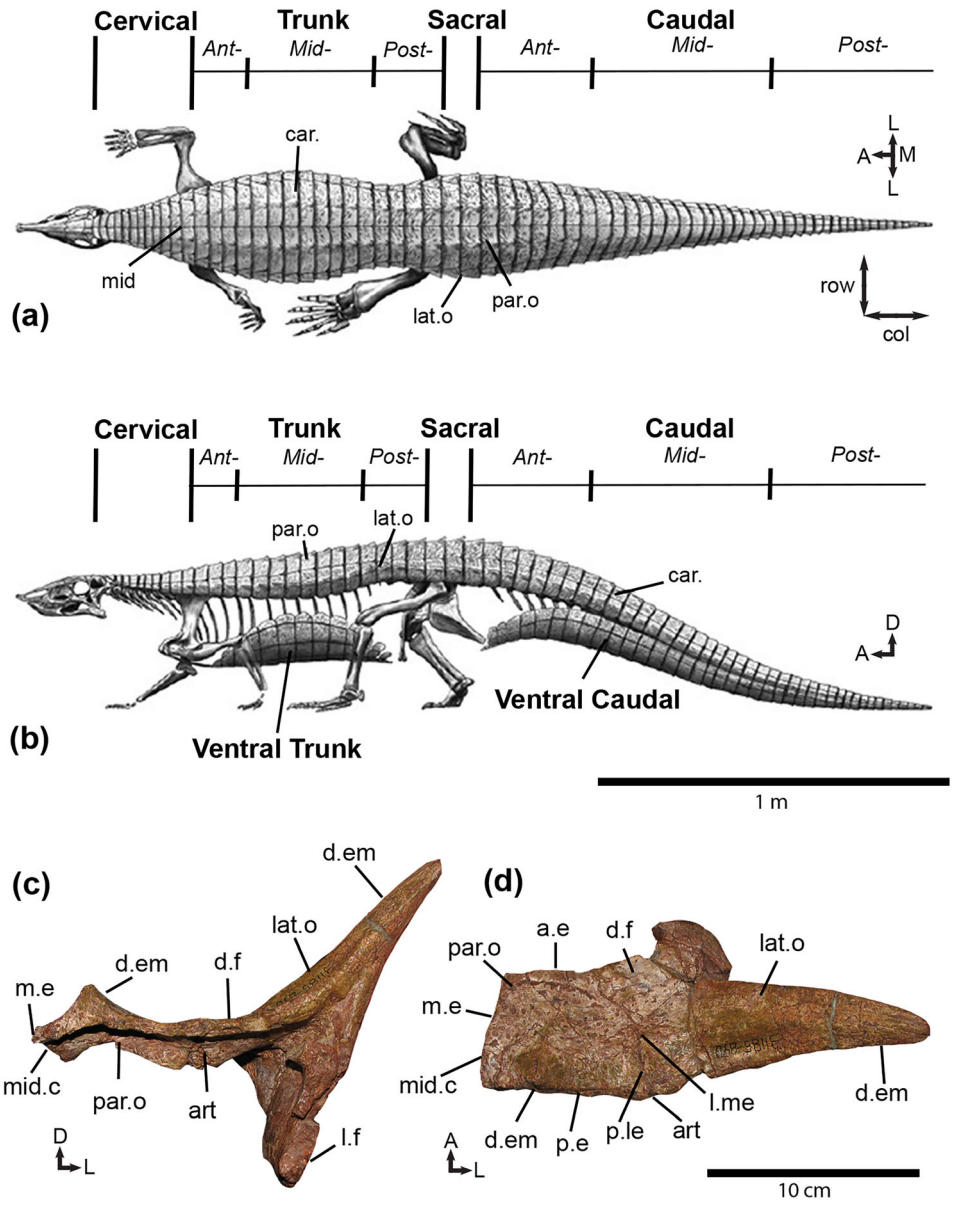

FIGURE 3 Differentiation, terminology, and directionality of aetosaur osteoderms. (a,b) Generalized aetosaurian body plan with divisions and subdivisions of the carapace as exemplified by the reconstruction of *Stagonolepis robertsoni* by co-author Jeffrey Martz. (c-d) General nomenclature of paramedian (c) and lateral (d) osteoderms as exemplified by articulated cervical paramedian and lateral osteoderms in *Longosuchus meadei* (TMM 31185-97). Figure modified from Parker (2016a) and Parker and Martz (2010). A, anterior; Ant, anterior-trunk; art, articulation between paramedian and lateral osteoderm; a.e, anterior edge; car, carapace; col, osteoderm columns; D, dorsal; d.f, dorsal flange; d.em, dorsal eminence; L, lateral; l.f, lateral flange; l.me, lateral osteoderm medial edge; lat.o, lateral osteoderm; M, medial; Mid-, mid-trunk; m.e, medial edge; mid.c, midline contact; mid, midline; p.e, posterior edge; p.le, paramedian lateral edge; par.o, paramedian osteoderm; Post-, posterior-trunk; row, osteoderm rows. Orientations: Dorsal: a,d; Left Lateral: b; Posterior: c. Arrows indicate anatomical direction.

in posterior view and straight lateral margin associated in the latter (e.g., UMMP 13950, *C. wellesi*, Case, 1932; Parker, 2018a); we interpret them as belonging to the posterior-half of the cervical region (Figure 3). Additionally, we interpret the paramedian osteoderms that exhibit a quadrangular crescentic shape in dorsal view as being derived from the anterior-trunk region (Figures 3 and 5; e.g., *T. coccinarum*, Martz, 2002, figure 4.26). The paramedian osteoderms in the cervical and anterior-trunk regions are dorsoventrally thin (Figures 4b and 5c), unlike those of *T. chatterjeei* (Martz & Small, 2006). Within these regions the paramedian osteoderms exhibit medial edges that are straight and share a simple contact with the pairing paramedian osteoderm (Figures 4e and 5a); the elements lack the thick ridge-and-groove interlocking pattern observed in the desmatosuchins *S. macalpini* (UMMP V60817, Parker et al., 2008), *L. hunti* (TMM 31185–66, Parker & Martz, 2010), *L. meadei*, and *Desmatosuchus* (Parker, 2005a, 2008). Where preserved, the anterior edge lacks the anterior bar that characterizes most aetosaur taxa (Desojo et al., 2013) and shared with nonaetosaur aetosauriforms (Marsh et al., 2020; Parker et al., 2021), nor is it characterized as a depressed anterior lamina (Figures 4e and 5a), a feature only described within *Desmatosuchus* and historically thought to be an apomorphy of the genus (Parker, 2005a, 2008, 2016a). Instead, it is characterized as a thin, smooth, unornamented strip of bone (Figures 4a and 5a). Because the anterior margins are not totally preserved, we are unable to unambiguously confirm the absence of scalloping or of an anteromedial process projecting anteriorly off the anterior edge of the paramedian osteoderm, features

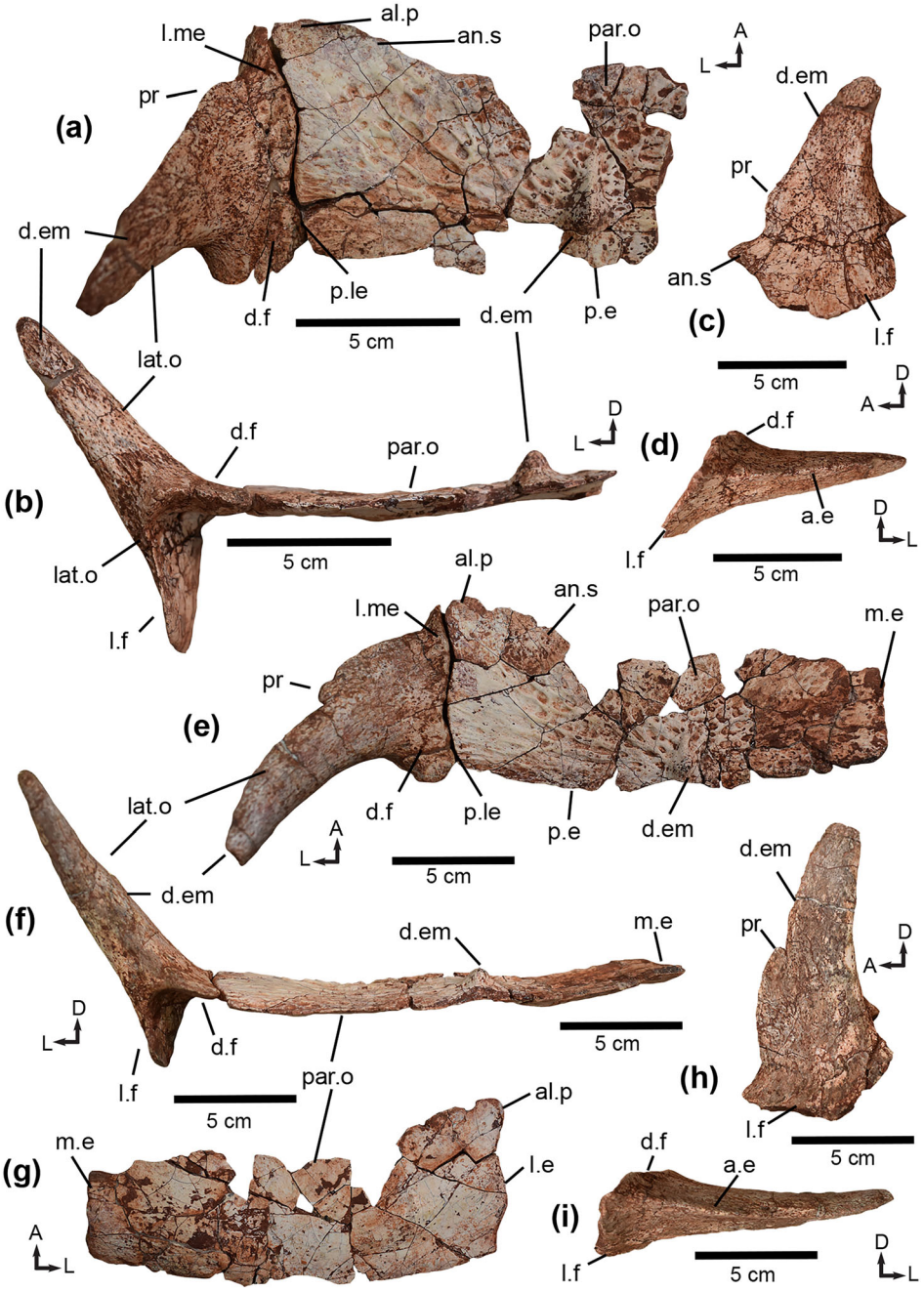

FIGURE 4 Cervical osteoderm morphology in *Garzapelta muelleri* gen. et sp. nov. (TTU-P 10449). (a,b,e,f) Paramedian and lateral osteoderms are figured in articulation, but they are disarticulated in TTU-P 10449. (c,d) Lateral osteoderm in (a,b). (h,i) Lateral and (g) paramedian osteoderm in (e,f). A, anterior; a.e, anterior edge; al.p, anterolateral process; an.s, anterior surface; D, dorsal; d.f, dorsal flange; d.em, dorsal eminence; L, lateral; l.f, lateral flange; l.e, lateral edge; l.me, lateral osteoderm medial edge; lat.o, lateral osteoderm; m.e, medial edge; pr, protuberance; p.e, posterior edge; p.le, paramedian osteoderm lateral edge; par.o, paramedian osteoderm. Orientations: Dorsal: a,d; Oblique Lateral: c, f; Anterior: d,i; Posterior: b,e; Ventral: g. Arrows indicate anatomical direction.

observed in *Scutarx deltatylus* (Parker, 2016b). The paramedian osteoderms exhibit a thin posterior edge (Figures 4b and 5a) and are not dorsoventrally thickened like those of *T. chatterjeei* (Martz & Small, 2006). The lateral edge is weakly sigmoidal and trends anteroposteriorly in the cervical region (Figure 4a); however, in the anterior-trunk region, the lateral edge becomes more posteromedially inclined (Figure 5a), and the posterior lateral edge takes on a beveled appearance in some paramedian osteoderms due to the dorsal flange of the lateral osteoderm projecting more strongly (Figure 5d,g). Additionally, in these regions the lateral edge forms a short, anterolaterally rounded process as it becomes confluent with the anterior edge (Figures 4a and 5d) similar to the condition observed in *Paratypothorax* (Long & Ballew, 1985; Martz et al., 2013), *T. chatterjeei* (Martz & Small, 2006), *T. coccinarum* (Long & Murry, 1995; Martz, 2002), *V. armatum* (Haldar et al., 2023), and in the narrow-bodied aetosaurs *A. scagliai* (Desojo & Ezcurra, 2011; Heckert & Lucas, 2002) and *A. ferratus* (Schoch, 2007). In the anterior-trunk region, the anterolateral process projects beyond the lateral edge and overlaps onto the anterior edge of the adjacent lateral osteoderm as in most aetosaurs (Figure 5), but unlike the condition observed in desmatosuchins where the lateral osteoderm instead overlaps the paramedian osteoderm (Figure 3d; Parker & Martz, 2010).

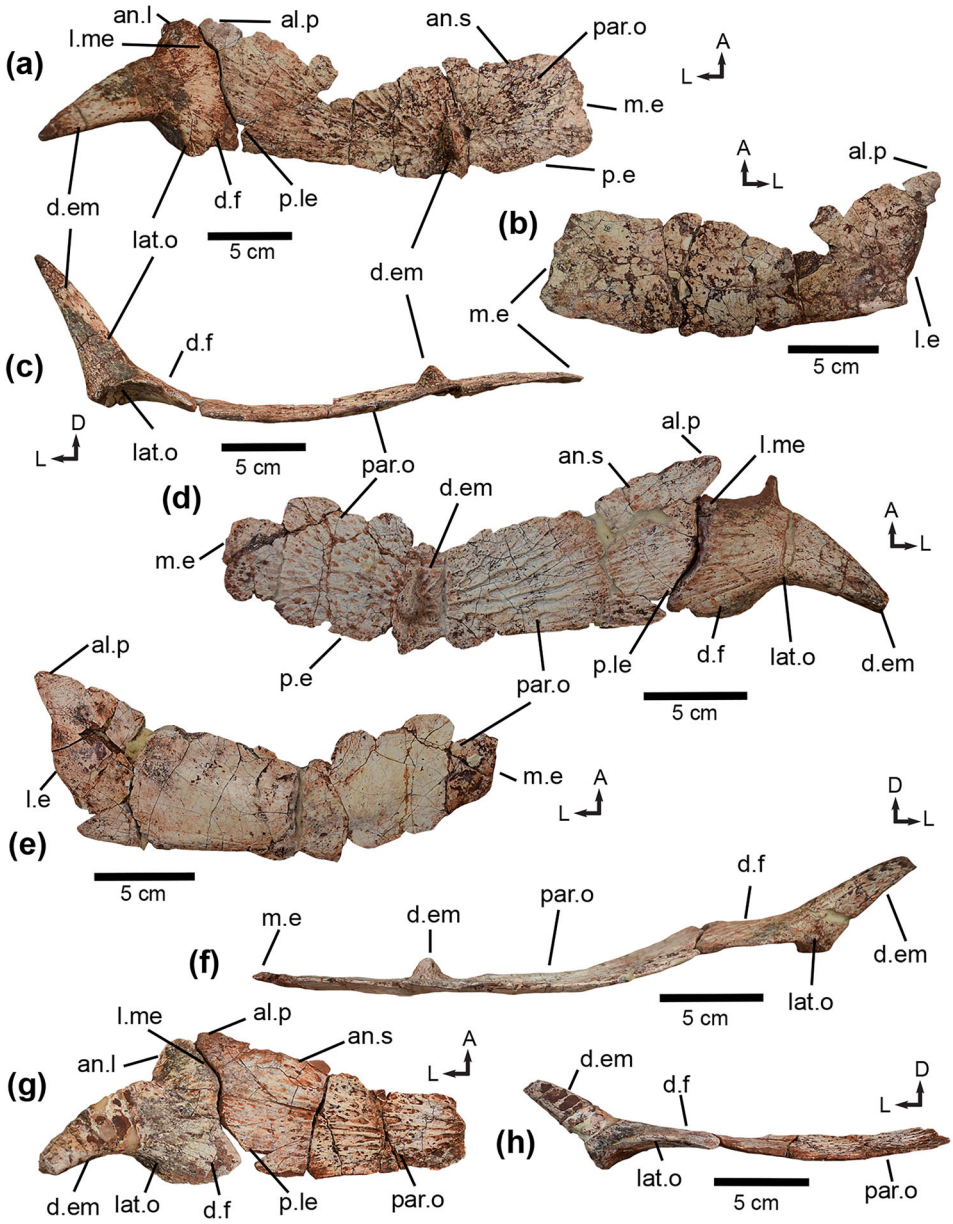

FIGURE 5 Anterior-trunk osteoderm morphology in *Garzapelta muelleri* gen. et sp. nov. (TTU-P 10449). (a,c,d,f–h) Paramedian and lateral osteoderms are figured in articulation, but they are disarticulated in TTU-P 10449. (b,e) Paramedian osteoderm in (a,c) and (d,f), respectively. a, anterior; al.p, anterolateral process; an.s, anterior surface; D, dorsal; d.f, dorsal flange; d.em, dorsal eminence; l, lateral; l.e, lateral edge; l.me, lateral osteoderm medial edge; lat.o, lateral osteoderm; m.e, medial edge; p.e, posterior edge; p.le, paramedian osteoderm lateral edge; par.o, paramedian osteoderm pr, protuberance. Orientations: Dorsal: a,d, g; Posterior: c,f,h; Ventral: b,e. Arrows indicate anatomical direction.

The cervical osteoderms of *G. muelleri* exhibit a weakly developed dorsal eminence that does not contact the posterior edge (Figure 4a), a condition shared with *L. hunti* (Parker & Martz, 2010), *Desmatosuchus* (Case, 1922; Parker, 2005a), *P. andressorum* (Long & Ballew, 1985; Martz et al., 2013; Martz & Small, 2006); this is unlike the well-developed eminence observed in *Gorgetosuchus pekinensis* (Heckert et al., 2015) or *R. chamaensis* (Parker, 2007) which lacks a dorsal eminence in the cervical osteoderms, a condition shared with most aetosaur taxa (Desojo et al., 2013). In the anterior-trunk region, the eminence is slightly more developed (Figure 5f). The dorsal eminence is low and sub-pyramidal with an anteriorly elongate keel (Figure 5a,c) similar to most desmatosuchins except *G. pekinensis* (NCSM 21723, Heckert et al., 2015) and *L. hunti* (Parker & Martz, 2010). The dorsal eminence is centralized in the cervical paramedian osteoderms (Figure 4e) and becomes slightly offset medially (Figure 5d) in the trunk region. The dorsal ornamentation is radiate (Figure 5d) as observed in most taxa (Desojo et al., 2013), but unlike the randomly pitted reticulate ornamentation observed in *T. coccinarum* (Heckert et al., 2010; Long & Murry, 1995; Martz, 2002) or the random ornamentation observed in *Desmatosuchus* (Case, 1922; Parker, 2005a, 2008). The radial ornamentation is composed of oblong-shaped pits that are oriented/inclined towards the anterolateral and anteromedial margins from the eminence (Figure 5d). Furthermore, these pits are separated by well-defined ridges that anastomose with each other (Figure 5d). There is no evidence of the long grooves or rays that are observed particularly along the posterior edge in the cervical and anterior-

trunk paramedian osteoderms of *Coahomasuchus* (Heckert et al., 2015; Heckert & Lucas, 1999), *Paratypothorax* (Long & Ballew, 1985; Martz et al., 2013), and *T. chatterjeei* (TTU-P 545, Martz & Small, 2006). The dorsal ornamentation starts off faint in the cervical region and becomes more incised in the trunk region (Figures 4e and 5d). Overall, the ornamentation is most similar to that of *R. chamaensis* (Parker, 2007) as originally noted by Martz (2008:pg. 212). In posterior view, the paramedian osteoderms derived from the anterior-trunk region exhibit a slight dorsally oriented curvature near the lateral edge (Figure 5f); this curvature is different from the ventral flexure/arching that is observed in some paramedian osteoderms at the center of ossification in the mid-trunk and caudal regions (e.g., *C. wellesi*, Case, 1932; Long & Ballew, 1985; Parker, 2018a). Although this might be taken for taphonomic distortion, the orientation of this flexure is continued by the adjacent lateral osteoderm and seen consistently in various paramedian osteoderms. The paramedian osteoderms show no evidence of a ventral strut, thus they are smooth and flat (Figures 4g and 5e). However, there are two nutrient foramina at the center of ossification (=location below the dorsal eminence; Parker, 2008); comparative studies on the osteoderms of the extant crocodyliform *Alligator mississippiensis* indicate that in life these foramina would have been infilled by vessels that provide blood supply to the osteoderm (Seidel, 1979, figures 1 and 2; Frey, 1988, figure 20).

5.1.2 | Mid-trunk region

TTU-P 10449 preserves a pair of lateral and paramedian osteoderm that we interpret as being derived from the mid-trunk region (Figures 3 and 6a–d). In this region the paramedian osteoderm exhibits a W:L of ~3.2. This ratio is similar to those of nondesmatosuchin stagonolepidoids (e.g., *C. wellesi*; Case, 1932; Parker, 2016a, 2018a; Reyes et al., 2023), but lower than those of most typothoracines (e.g., *T. coccinarum*, Martz, 2002; Heckert et al., 2010) in which the widest paramedian osteoderms exhibit a W:L of 3.5 or greater. In dorsal view, the paramedian osteoderm is anteroposteriorly broader than those in the anterior-trunk region and not as crescentic (Figure 6a). The dorsal ornamentation is composed of moderately incised grooves and anastomosing ridges that radiate from the dorsal eminence; however, there is no evidence of the long rays/grooves observed in *Coahomasuchus* (Heckert et al., 2015; Heckert & Lucas, 1999) and *Paratypothorax* sp. (Long & Ballew, 1985; Lucas et al., 2006; Martz et al., 2013). The dorsal eminence remains a low, medially offset, anteriorly keeled, and pyramidal-shaped structure that does not contact the posterior border of the osteoderm (Figure 6a). The posterior edge lacks the beveling observed in the mid-trunk paramedian osteoderms of *T. chatterjeei*, *Paratypothorax* (Martz et al., 2013; Martz & Small, 2006), *K. sylvestris* (Czepiński et al., 2021), and *V. armatum* (Haldar et al., 2023). The anterior margin of the paramedian osteoderm is not fully preserved, but it is evident that the element exhibited a thin, smooth, unornamented strip of bone (Figure 6a) rather than an anterior bar or depressed lamina, similar to the condition observed in the preceding region. The anterior margin of this osteoderm is scalloped (Figure 6a); however, close examination indicates that this is a taphonomic feature as the anterior margin is not completely preserved. Accordingly, we are unable to confirm the presence or absence of scalloping in the mid-trunk paramedian osteoderms of TTU-P 10449. The anteromedial corner is not preserved, so we are unable to determine if it exhibits an anteriorly projecting triangular process as observed in *A. scagliai* (Heckert & Lucas, 2002), *C. wellesi* (Parker, 2018a) or paratypothoracins (Martz & Small, 2006; Parker, 2007). Similarly, the anterolateral corner is not preserved; however, the adjacent lateral osteoderm (Figure 6a) indicates that the paramedian osteoderm exhibits a rounded anterolateral process with a slight dorsolateral inclination that does not project far beyond the lateral margin similar to typothoracines (e.g., *T. coccinarum*, Long & Murry, 1995; Martz, 2002; Parker, 2016a), *A. scagliai* (Heckert & Lucas, 2002), and *A. ferratus* (Schoch, 2007). In the mid-trunk region, the lateral margin is more anteroposteriorly oriented (Figure 6a) than those in the anterior-trunk region (Figure 5a), which has a more posteromedial inclination towards the posterior margin. The lateral margin is broad, weakly sinuous, and laterally convex for most of its contact with the adjacent lateral osteoderm. It remains slightly concave near the posterior border but is unlike the "cutoff" corner described in *Adamansuchus eisenhardtae* (Lucas, 2007) and paraypothoracins (e.g., *Paratypothorax* sp., TTU-P 9169; Martz et al., 2013).

In posterior view, the paramedian osteoderm is dorsoventrally thin (Figure 6b) similar to those of *Paratypothorax* sp. (TTU-P 9169; Long & Murry, 1995; Martz et al., 2013), but unlike those of *T. chatterjeei* (Martz & Small, 2006) and *K. caerula* (Reyes et al., 2023) which are dorsoventrally thick. The paramedian osteoderm is predominantly transversely flat; however, it gradually curves dorsally for most of its lateral extent (Figure 6b). This condition is noted in the anteriortrunk region (Figure 5f); however, it is more dorsally pronounced in the mid-trunk region. This is one of the main features that distinguishes paramedian osteoderms from the mid-trunk region. This dorsolateral flexure of the paramedian osteoderm is only documented, but not formally described, within *Paratypothorax* (Long & Ballew, 1985; Long & Murry, 1995; Lucas et al., 2006; Martz et al., 2013). In ventral view, the ventral

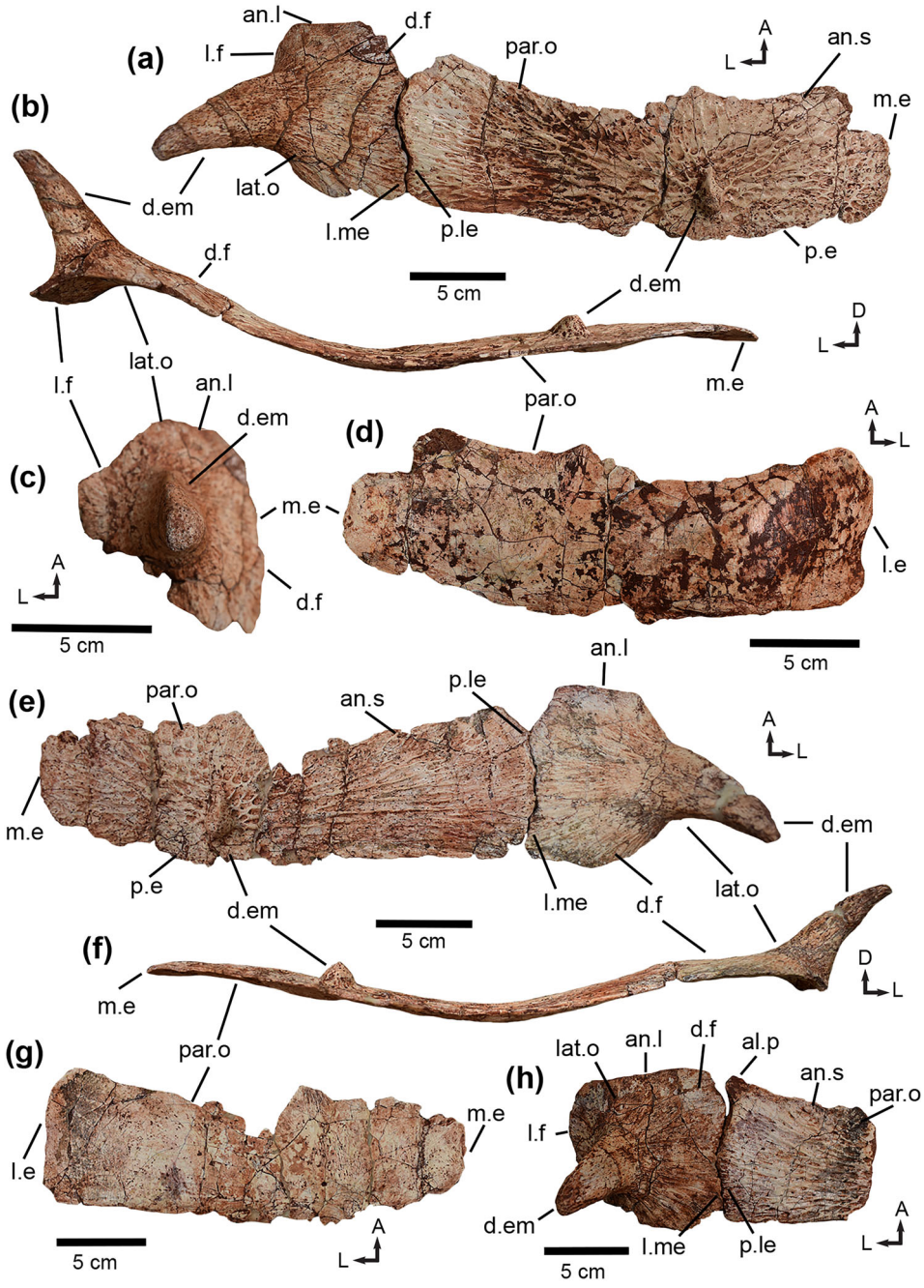

FIGURE 6 Mid-trunk (a–d), Posterior-trunk and sacral osteoderm (e–h) morphology in *Garzapelta muelleri* gen. et sp. nov. (TTU-P 10449). (a,b,e,f,h) Paramedian and lateral osteoderms are figured in articulation, but they are disarticulated in TTU-P 10449. (d,g) Paramedian osteoderm in (a,b) and (e,f), respectively. a, anterior; al.p, anterolateral process; an.s, anterior surface; d, dorsal; d.f, dorsal flange; d.em, dorsal eminence; l, lateral; l.f, lateral flange; l.e, lateral edge; l.me, lateral osteoderm medial edge; lat.o, lateral osteoderm; m.e, medial edge; p.e, posterior edge; p.le, paramedian osteoderm lateral edge; par.o, paramedian osteoderm. Orientations: Dorsal: a,e,h; Posterior: b,f; Ventral: d,e; Oblique lateral: c. Arrows indicate anatomical direction.

surface of the paramedian osteoderm is predominantly smooth, lacking the ventral strut similar to desmatosuchins (e.g., *Desmatosuchus*; Parker, 2005a, 2008, 2016a), and exhibits longitudinal striations on the posterior portion of the osteoderm where it overlaps the anterior bar of the proceeding osteoderm; additionally, nutrient foramina at the center of ossification (Figure 6d).

5.1.3 | Posterior-trunk and sacral regions

TTU-P 10449 preserves a relatively complete paramedian osteoderm (Figure 6e,f) that we interpret as being derived from the posterior-trunk and/or sacral regions (Figure 3) based on its larger anteroposterior length and transverse width. The articulated carapaces of several aetosaur taxa (e.g., *C. wellesi*, *C. kahleorum*, *T. coccinarum*, *D. spurensis*; Case, 1922, 1932; Heckert et al., 2010; Heckert & Lucas, 1999; Parker, 2008, 2018a) indicate that paramedian osteoderms within the posterior-trunk and sacral regions are similar in morphology. In general, the paramedian osteoderm derived from the posterior-trunk and/or sacral regions in TTU-P 10449 exhibit a similar morphology to those derived from the mid-trunk region with a W:L of ~3.3 and are anteroposteriorly broad. The anterior edge is not fully preserved but it is evident that it

is a flat, smooth strip of bone devoid of ornamentation (Figure 6d), as observed in described in the preceding regions of the dorsal carapace. Although the anterolateral process is not preserved, the pairing lateral osteoderm indicates that the anterolateral process is rounded with an anterolateral inclination that does not project far beyond the lateral edge (Figure 6e); a fragmentary paramedian osteoderm that pairs with what we interpret to be a sacral lateral osteoderm (Figure 6h), indicates the anterolateral process does support the interpretation above. The dorsal eminence is medially offset, positioned anterior to the posterior edge, and pyramidal-shaped with an anterior keel; however, it is more prominent and dorsally projecting than those in the mid-trunk region (Figure 6e,f). The dorsal ornamentation remains composed of deeply incised grooves and anastomosing ridges that radiate from the dorsal eminence. The medial edge is anteroposteriorly straight (Figure 6e). The anteromedial and posteromedial corners are not fully preserved. The osteoderms are dorsoventrally thin (Figure 6f), with no indication of becoming thicker and more robust into the pelvic region of the carapace. There is no evidence of a beveled posterior margin, unlike the condition observed in *Paratypothorax* (Long & Ballew, 1985; Lucas et al., 2006; Martz et al., 2013) and *T. chatterjeei* (Martz & Small, 2006). This suggests that the beveled margin is absent in the carapace of TTU-P 10449. In dorsal view, the paramedian osteoderms are slightly crescentic (Figure 6e) similar to those of the mid-trunk region. Additionally, there is no evidence of a ventral strut on the ventral surface of the paramedian osteoderm, but there are foramina present at the center of ossification (Figure 6g).

Although the paramedian osteoderms derived from the posterior-trunk and sacral regions are similar to those from the mid-trunk region in TTU-P 10449, they do exhibit notable differences that differentiate them from each other. In the posterior-trunk the lateral margin is anteroposteriorly broad and characterized as a laterally oriented convex edge posterior of the anterolateral process (Figure 6e). The morphology of the lateral edge is similar to the condition observed in a trunk paramedian osteoderm of *R. chamaensis* (NMMNH P-35807, Parker, 2007). However, in the sacral region the lateral margin is not broadly convex as described above (Figure 6h). Additionally, in posterior view, the paramedian osteoderms exhibit an upwards curvature near the lateral margin (Figure 6f). However, it is less upturned than the paramedian osteoderms of the mid-trunk region (Figure 6b). Instead, it resembles those of the anterior-trunk region (Figure 5f) indicating that this upwards curvature is most prominent in the mid-trunk region and gradually reduces into the posterior-trunk and sacral regions.

5.1.4 | Anterior-caudal region

Several paramedian osteoderms preserved in TTU-P 10449 are derived from the anterior-caudal region (Figures 3 and 7); these elements vary in preservation with most exhibiting a broken anterior edge. The widest preserved paramedian osteoderms exhibit an average W:L of ~3.1, less than those in the mid- and posterior-trunk regions; the W:L decreases gradually into the mid-caudal region. In general, the morphology of paramedian osteoderms from the anterior-caudal region is similar to those preceding them. The osteoderms are dorsoventrally thin with no evidence of a beveled posterior margin (Figure 7e). The dorsal ornamentation is radiate and well-incised (Figure 7a). The dorsal eminence is dorsally projecting, medially offset, does not contact the posterior margin, and is pyramidal-shaped with an anterior keel, but more developed than those in the preceding regions (Figure 7f,g); it is evident the dorsal eminence does not develop into an elongate spine as observed in the pelvic region of *R. chamaensis* (Parker, 2007). The dorsal eminence becomes gradually positioned closer to the medial edge posteriorly down the anterior-caudal region. Anteriorly, the paramedian osteoderms still exhibit an anterior edge that is dorsoventrally thin, smooth, and devoid of ornamentation (Figure 7a). The medial edge is anteroposteriorly straight with a quadrangular posteromedial corner (Figure 7f); the margins of the anteromedial corner do not appear to be fully preserved. TTU-P 10449 preserves a right paramedian osteoderm that exhibits an abnormal indentation of the anterior margin medial to the dorsal eminence, so that the medial part of the osteoderm is anteroposteriorly shorter than the portion lateral to the dorsal eminence (Figure 7d). This condition also occurs in a paramedian osteoderm of *S. deltatylus* (PEFO 31217) that exhibits abnormal indentations in both anterolateral and posteromedial corners. This feature is uncharacteristic of most aetosaur paramedian osteoderms, which exhibit a quadrangular medial portion (Desojo et al., 2013; Parker, 2016a). Thus, we hypothesize that this condition is pathological in origin and possibly a result of incomplete ossification of the paramedian osteoderm (Figure 7d).

Although similar in morphology to those in the trunk region, the paramedian osteoderms of the anterior-caudal region exhibit notable differences. The posterior margin is not horizontally straight in dorsal view (Figure 7a); instead, it is sinuous, being scalloped (i.e., anteriorly convex) both medial and lateral to the dorsal eminence (Figure 7a). This results in a posteriorly oriented tongue-like extension of the posterior edge directly posterior of the dorsal eminence (Figure 7a). This morphology of the posterior edge has been otherwise described only in a

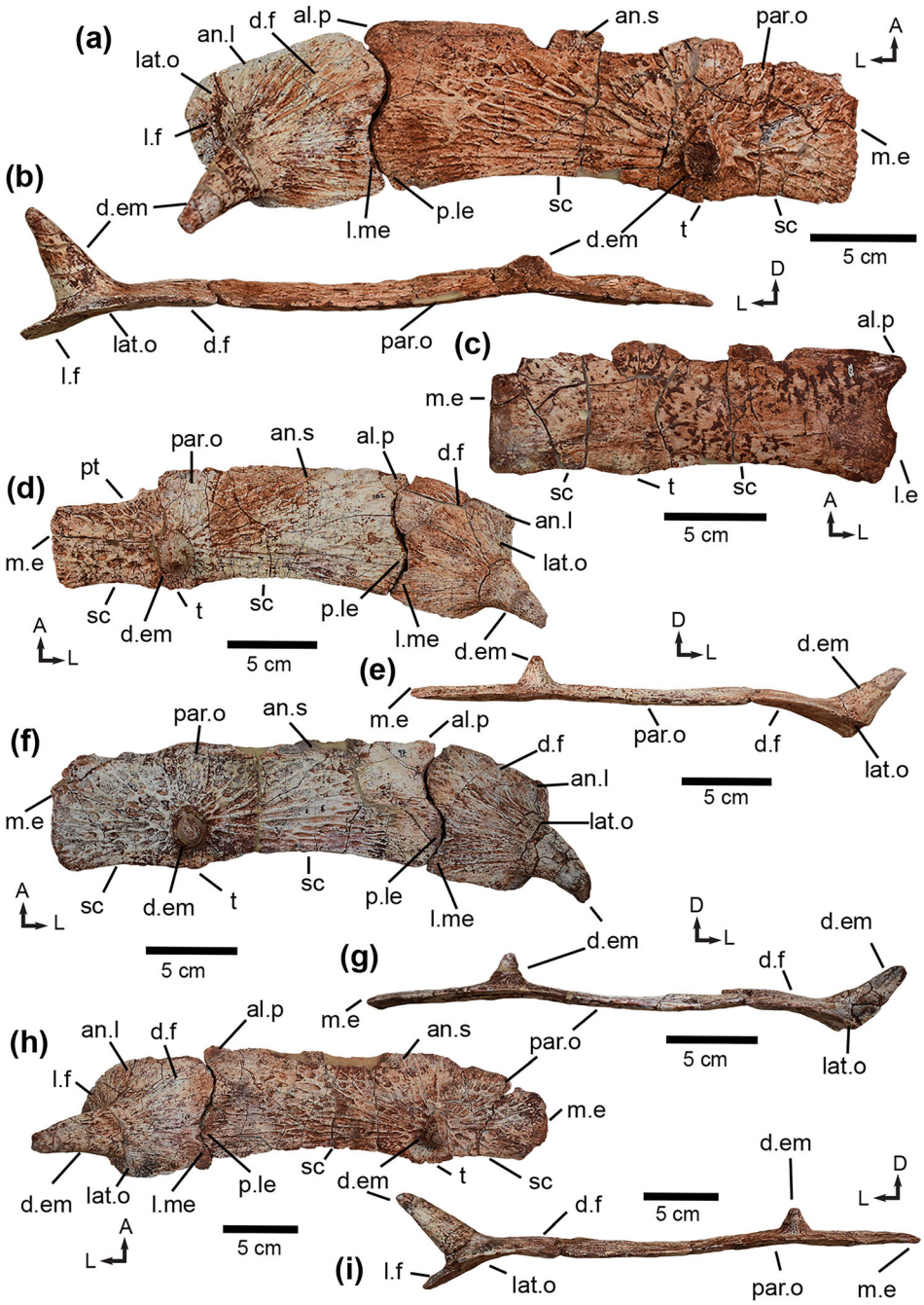

FIGURE 7 Anterior-caudal osteoderm morphology in *Garzapelta muelleri* gen. et sp. nov. (TTU-P 10449). (a,b,d–i) Paramedian and lateral osteoderms are figured in articulation, but they are disarticulated in TTU-P 10449. (c) Paramedian osteoderm in (a,b). a, anterior; al.p, anterolateral process; an.s, anterior surface; d, dorsal; d.f, dorsal flange; d.em, dorsal eminence; L, lateral; l.f, lateral flange; l.e, lateral edge; l.me, lateral osteoderm medial edge; lat.o, lateral osteoderm; m.e, medial edge; pt, pathology; p.le, paramedian osteoderm lateral edge; par.o, paramedian osteoderm; sc, scallop; t, tongue-like projection. Orientations: Dorsal: a,d,f,h; Posterior: b,e,g,i; Ventral: C. Arrows indicate anatomical direction.

trunk paramedian osteoderm of *R. chamaensis* (NMMNH P-33820; Parker, 2007). In the anterior-trunk region, the lateral margin of the paramedian osteoderms is strongly sigmoidal (Figure 7a) to an extent not observed in any currently described taxon suggesting that this condition is an autapomorphy of *G. muelleri*. The lateral margin is deeply concave just posterior to the anterolateral process and becomes broadly laterally convex posteriorly, gradually becoming confluent with the posterior edge (Figure 7a). In dorsal view, the anterolateral process is characterized as a short, rounded, and does not project beyond the lateral margin (Figure 7a); they are reduced in comparison to those from the trunk region. In posterior view, the paramedian osteoderms of the anterior-caudal region are transversely straight and do not exhibit the upward curvature of the lateral margin observed in the trunk region (Figure 7e). This gradual decrease in the lateral upward curvature of the paramedian osteoderm is observed in *Paratypothorax* sp. (PEFO 3004).

TTU-P 10449 also preserves a right paramedian osteoderm (Figure 8a–c) that is derived from the posteriormost rows of the anterior-caudal region. This osteoderm is similar to those preceding it but exhibits clear distinctions in morphology. The posterior margin is fragmented

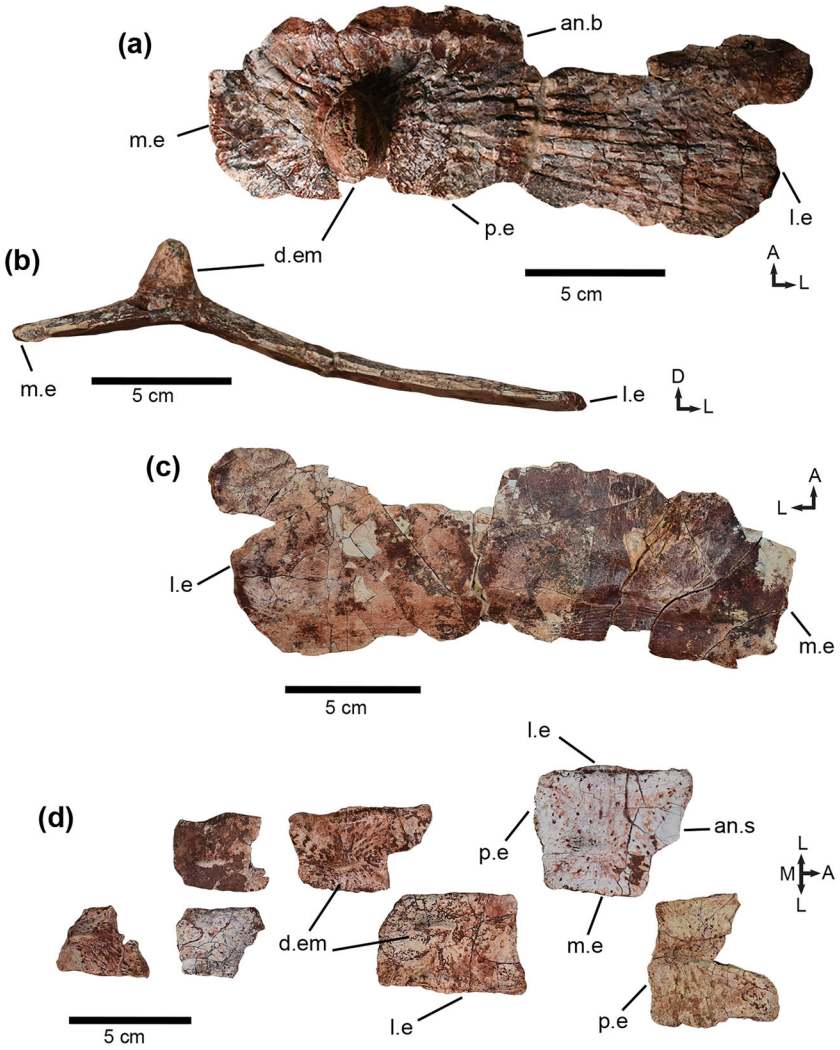

FIGURE 8 Anterior- (a–c) and posterior-caudal (d) osteoderm morphology in *Garzapelta muelleri* gen. et sp. nov. (TTU-P 10449). A, anterior; an.b, anterior bar; D, dorsal; d.em, dorsal eminence; L, lateral; l.e, lateral edge; M, medial; m.e, medial edge; p.e, posterior edge. Orientations: Dorsal: a,d; Posterior: b; Ventral: c. Arrows indicate anatomical direction.

but it is apparent that it was horizontally straight (Figure 8a), lacking the scalloping and posteriorly oriented tongue-like extension that is observed in the paramedian osteoderms that precede it in the anterior-caudal region (Figure 7). The lateral edge is weakly sigmoidal and tapers posteromedially (Figure 8a). The anterolateral process is not fully preserved, but it appears to be reduced in its prominence; this reduction of the anterolateral process is also observed in *C. wellesi* (UMMP 13950; Parker, 2018a) and *Paratypothorax* sp. (PEFO 3004; Lucas et al., 2006). In posterior view, the paramedian osteoderm exhibits a strong ventral flexure that originates at the center of ossification (Figure 8b). This flexing of the osteoderm is associated with the transverse curvature of the tail. The dorsal eminence maintains the same general morphology described in the more anteriorly positioned paramedian osteoderms. However, it is more robust and well-developed, taking on a slightly more conical appearance and being positioned closer to the medial edge (Figure 8b). A key feature of this osteoderm is that the anterior edge exhibits a weakly developed anterior bar that is moderately developed on the medial half of the osteoderm and gradually thins laterally into a smooth surface (Figure 8a); a feature that is not present in the preceding paramedian osteoderms preserved in TTU-P 10449, which exhibit a thin, smooth, strip of bone devoid of ornamentation. A weekly developed anterior bar is shared with the paratypothoracins *R. chamaensis* (Parker, 2007), *Paratypothorax* sp. (Lucas et al., 2006), *V. armatum* (Haldar et al., 2023), and *K. sylvestris* (Czepiński et al., 2021). The presence of this weakly developed anterior bar indicates that this feature develops abruptly in the anterior caudal region of TTU-P 10449. Currently, TTU-P 10449 is the only aetosaur to show variation of its anterior edge between the pre and postcaudal regions of the dorsal carapace.

5.1.5 | Posterior-caudal region

TTU-P 10449 preserves several paramedian osteoderms that are small and quadrangular, being anteroposteriorly

longer than transversely wide (Figure 8d). Their morphology indicates that they are derived from the dorsal posterior-caudal region (Figure 3). The paramedian osteoderms lack the weakly developed anterior bar described above, instead they exhibit an anterior edge that is thin, smooth, and devoid of ornamentation as observed in the precaudal region. Additionally, they exhibit a faint radial ornamentation with an eminence that is characterized as an anteroposteriorly oriented low keel that does not contact the posterior edge and becomes more reduced and positioned closer to the medial edge. (Figure 8d); reduction of the dorsal eminence and weakening of the ornamentation is seen in the more posterior paramedian osteoderms of other aetosaurs (e.g., Martz, 2002). Additionally, these paramedian osteoderms taper posteriorly, consistent with the narrowing of the tail. These paramedian osteoderms lack the anterolateral process and exhibit anteroposteriorly straight medial and lateral edges (Figure 8d), although the lateral edge exhibits an embayment for the contact with the adjacent lateral osteoderm.

5.2 | Lateral osteoderms

TTU-P 10449 preserves a total of 34 lateral osteoderms that span most of the preserved carapace, except for the mid- and posterior-caudal region (Figure 3). Because several of these osteoderms articulate with the associated paramedian osteoderms, we can use our interpretations of the relative positioning of the paramedian osteoderms (described above) as a proxy to determine the region from which the lateral osteoderms are derived. This allows us to describe the morphology of the associated lateral osteoderms in TTU-P 10449 in a relative sequence across the various regions of the dorsal carapace (Figure 3).

5.2.1 | Cervical and anterior-trunk regions

Lateral osteoderms derived from the cervical region (Figure 4a–d) are strongly asymmetrical with the lateral flange being transversely wider than the dorsal flange, which is reduced. However, beginning in the anterior-trunk region (Figure 5g,h), the asymmetry is reversed with the dorsal flange being transversely wider than the lateral flange, which is highly reduced in comparison. This transition in asymmetry is observed in the desmatosuchins *D. spurensis* (MNA V9300, Parker, 2008), *Sierritasuchus macalcapini* (UMMP V60817, Parker et al., 2008), and *L. meadei* (TMM 31185-84, Sawin, 1947). These taxa indicate that in the cervical-anterior trunk region, the dorsal flange starts off reduced in comparison to the lateral flange, grows proportionately larger until it equals the lateral flange in length, and then becomes proportionately larger than the lateral flange. This is likely also the case in *G. muelleri*; however, TTU-P 10449 does not preserve a transitional lateral osteoderms where the flanges are equal in size (Figures 4 and 5); this state is exemplified by an isolated lateral osteoderm *Sierritasuchus macalpani* (TTU-P 10731, Parker et al., 2008, figure 5b) and *G. pekinensis* (NCSM 21723, Heckert et al., 2015). The anterior edge of the lateral osteoderm is characterized by as a predominantly smooth strip of bone (Figure 4a), as observed in most of the preserved paramedian osteoderms; however, this region is anteroposteriorly thinner than that observed in the adjacent paramedian osteoderm. In general, the dorsal eminence is a well-developed, posteriorly recurved spine that is of moderate length (Figure 4b,e) similar to the condition observed in most desmatosuchins (Figure 3c,d; e.g., *L. meadei*, TMM 31185-97; Parker, 2016a; Parker & Martz, 2010; Sawin, 1947) but unlike the large, elongated horns in *Desmatosuchus* (Long & Murry, 1995; Martz et al., 2013; Parker, 2005a, 2008). Additionally, these spines are unlike the dorsoventrally flattened spines observed in typothoracines (e.g., *T. coccinarum*, NMMNH P-56299, Heckert et al., 2010), or the low elongate keels that characterize most aetosaur taxa (e.g., *C. kahleorum*, NMMNH P-18496, Heckert & Lucas, 1999; TMM 31100–437). The spine grows proportionately larger down the cervical series into the anterior-trunk region (Figures 4 and 5) and becomes more centralized away from the medial edge of the lateral osteoderm. Anteriorly, the spine exhibits a slightly compressed keel that originates at the base and extends to the apex, and a protuberance near the base (Figure 4c,d,h–i); the development of this protuberance varies across the cervical region, where it can be characterized as a low swelling (Figure 4c) or as strongly protruding (Figure 4h). This protuberance is not present in the cervical lateral osteoderms of other taxa that exhibit a similar spine to TTU-P 10449 suggesting that this is an autapomorphy of *G. muelleri*. However, a similar condition has been noted, although not formally described, in the pelvic lateral osteoderms of *T. coccinarum* (NMMNH P-56299) and *Paratypothorax* sp. (PEFO 3004, Parker, 2007, figure 8e). In *T. coccinarum* the anterior edge of the spine exhibits a slight swelling of the bone surface, while in *Paratypothorax* sp. the swelling is more developed almost resembling the protuberance described here for TTU-P 10449. Additionally, the spines of TTU-P 10449 lack the posterior embayment (Figure 4b and 5c) observed in *L. meadei* (Figure 3c; TMM 31185-97, Parker & Martz, 2010; Sawin, 1947), *S. macalpini* (UMMP V60817, Parker et al., 2008), and typothoracines (Martz, 2002; Parker, 2016a), and is inclined laterally 45° from the sagittal plane (Figure 4b); however, the spine becomes

more laterally inclined transitioning into the mid-trunk region (Figure 5f).

In posterior view, the dorsal and lateral flanges exhibit a ~90° flexure between each other in the cervical region (Figure 4b,f) similar to *L. meadei* (Figure 3c) and *L. hunti* (Parker & Martz, 2010); however, the angle of flexure between two flanges gradually broadens in the anterior-trunk region (Figure 5c,f,h). In the cervical region, the dorsal flange is anteroposteriorly broad but less than half the transverse width of the lateral flange (Figure 4a,b). The medial edge of the lateral osteoderm is sigmoidal and exhibits a laterally inclined incision anteriorly for the overlap of the anterolateral process of the adjacent paramedian osteoderm (Figure 5a); unlike the reversed condition observed in desmatosuchins in which the dorsal flange of the lateral osteoderm is an anteromedial projection that overlaps the anterior edge of the paramedian osteoderm (Figure 3d; Parker, 2016a; Parker & Martz, 2010). The medial edge lacks the thickened tongue-and-groove interlocking contact with the paramedian osteoderm that is observed in desmatosuchins (Heckert et al., 2015; Parker, 2005a, 2008; Parker et al., 2008; Parker & Martz, 2010).

Although small in the cervical region, the dorsal flange of the lateral osteoderm expands in transverse width in the anterior trunk region and exhibits a more triangular, posteromedially projecting outline in dorsal view (Figure 5a,g); this is somewhat similar to typothoracines (Martz, 2002), in which the dorsal flange articulates with the "beveled" posterolateral edge of the paramedian. The dorsal flange continues to expand into the mid-trunk, pelvic, and anterior-caudal regions (Figures 5 and 7). The dorsal flange becomes anteroposteriorly longer caudally down the dorsal carapace, similar to the paramedian osteoderms. In the cervical region, the lateral flange is transversely wider than the dorsal flange (Figure 4a,b) and is semicircular in lateral view (Figure 4c). However, the lateral flange becomes reduced in comparison to the dorsal flange and takes on a semicircular shape in the anterior-trunk region (Figure 5h). The dorsal ornamentation is composed of elongate grooves radiating from the dorsal eminence (Figures 4c and 5d); the ornamentation is weakly incised in the cervical region (Figure 4c) in comparison to the anterior-trunk region (Figure 5d). The medial surface of the lateral osteoderm is smooth and perforated by two nutrient foramina at the center of ossification (=location of the dorsal eminence; Parker, 2008).

5.2.2 | Mid-trunk region

The lateral osteoderms of the mid-trunk region are similar to those in the anterior trunk region. The dorsal eminence remains a moderately developed, anteriorly keeled, posteriorly recurved spine that is positioned anterior of the posterior margin (Figure 6a,b) as observed in desmatosuchins (Heckert et al., 2015; Long & Murry, 1995; Parker, 2008; Parker et al., 2008; Parker & Martz, 2010); this is unlike the dorsoventrally compressed horn exhibited by typothoracines (Heckert et al., 2010; Martz, 2002; Martz & Small, 2006; Parker, 2007, 2016a) or low keeled eminence that is exhibited by nontypothoracine aetosaurines and nondesmatosuchin stagonolepidoids (e.g., *A. scagliai*, PVL 2073, Casamiquela, 1961, Desojo & Ezcurra, 2011, Heckert & Lucas, 2002, Parker, 2016a). Additionally, the spine lacks the posterior embayment observed in *L. meadei* (Parker & Martz, 2010) and no longer exhibits the anterior protuberances documented in the cervical and anterior-trunk regions (Figures 4 and 5). The spine is positioned closer to the ventrolateral edge instead of the dorsomedial edge. The dorsal flange is broad, rectangular, and more transversely expanded in dorsal view (Figure 6a) similar to *Desmatosuchus* (Case, 1932; Parker, 2005a, 2005b; Parker, 2008); it is unlike the triangular-shaped dorsal flanges observed in *C. wellesi* (Parker, 2018a) or highly reduced triangular flange in paratypothoracins (e.g., *T. chatterjeei*, Martz & Small, 2006). This results in a strongly asymmetrical lateral osteoderm with a large dorsal flange and reduced lateral flange. The lateral flange exhibits a semi-circular outline (Figure 6c); this is unlike the large, triangular lateral flange observed in *C. wellesi* (UMMP 13950; Case, 1932; Parker, 2018a), *S. deltatylus* (PEFO 34045; Parker, 2016b), and paratypothoracins (Martz et al., 2013; Martz & Small, 2006; Parker, 2005b, 2016a).

The medial edge is sigmoidal (Figure 6a); however, the anteromedial corner is not fully preserved. It is apparent that it exhibited an anterolateral inclined incision for the reception of the anterolateral process from the adjacent paramedian osteoderm. Anteriorly, the lateral osteoderm exhibits a thin, smooth surface with slight participation of the radial ornamentation (Figure 5). In posterior view, the dorsal and lateral flanges exhibit an obtuse flexure (Figure 6b) similar to nondesmatosuchin stagonolepidoids (e.g., *C. wellesi*, Case, 1932; Parker, 2018a) and nontypothoracine aetosaurines (e.g., *A. ferratus*, Schoch, 2007). This is unlike the 90° flexure observed in desmatosuchins (e.g., *D. spurensis*, Parker, 2008) or the highly acute lateral osteoderms observed in typothoracines (e.g., *T. coccinarum*, Martz, 2002). The dorsal spine is laterally inclined 45° from the sagittal plane. Additionally, the dorsal ornamentation is well incised and composed of grooves and ridges radiating from the spine (Figure 6a); the ornamentation is continued from the paramedian osteoderm onto the dorsal flange of the lateral osteoderm. The medial surface (=ventral in

articulation) of the lateral osteoderm is smooth and perforated by two foramina at the center of ossification. In sequence, the lateral osteoderms continue to gradually expand anteroposteriorly into the posterior-trunk region.

5.2.3 | Posterior-trunk and sacral regions

The preservation of the pelvic region of the carapace across several aetosaur taxa indicates that lateral osteoderms can vary in their morphology in the trunk-to-sacral transition (Figure 3) as observed in *C. wellesi* (PEFO 46222, UMMP 13950, Parker, 2018a), or remain uniform as observed in *C. kahleorum* (NMMNH P-18496; Heckert & Lucas, 1999; TMM 31100-437). Our interpretations on the relative positioning of the paramedian osteoderms in TTU-P 10449 suggest that the lateral osteoderms derived from the posterior-trunk and sacral regions vary in morphology (Figure 6). The lateral osteoderm derived from the posterior-trunk region (Figure 6e,f) is similar to those of the mid-trunk region. The only notable difference is that the medial edge exhibits a laterally oriented, broad, concave margin that contacts the broadly convex lateral margin of the adjacent paramedian osteoderm (Figure 6e). In comparison, the lateral osteoderm hypothetically derived from the sacral region (Figure 6h) is anteroposteriorly broader, with a sigmoidal medial edge that is not broadly concave, and more obtusely flexed than those in the preceding regions, allowing it to lay nearly flat on a horizontal plane. The dorsal flange remains broadly rectangular (Figure 6e,h), resulting in a strongly asymmetrical lateral osteoderm, where the lateral flange is broad, rectangular, and highly reduced. The dorsal eminence remains a moderately developed, anteriorly keeled, posteriorly recurved spine that does not contact the posterior border of the lateral osteoderm (Figure 6e,h). The anteromedial corner exhibits an anterolaterally inclined incision for the reception of the anterolateral process of the adjacent paramedian osteoderm (Figure 6e,h). The dorsal ornamentation remains well incised and composed of elongated grooves and ridges radiating from the dorsal spine.

5.2.4 | Anterior-caudal region

Most of the lateral osteoderms preserved in TTU-P 10449 are derived from the anterior-caudal region (Figures 3 and 7). The lateral osteoderms of the anterior-caudal region are asymmetrical with a dorsal flange that is approximately twice as transversely wide as the lateral flange (Figure 7a); this is unlike typothoracines which exhibit the inverse condition (Martz, 2002; Parker, 2007). The dorsal flange is anteroposteriorly shorter than those in the trunk and sacral region, indicating a gradual shortening of the anteroposterior length of the dorsal flange. Additionally, the transverse width of the dorsal flange reduces gradually posteriorly in the caudal region. In dorsal view, the dorsal flange remains quadrangular as observed in the preceding regions (Figure 7a) as observed in *D. spurensis* (Parker, 2008). Although reduced, the lateral flange is semicircular similar to those of *Paratypothorax* and *R. chamaensis* (Parker, 2007, figure 9); this is unlike the rectangular-shaped lateral flanges in *Desmatosuchus* (Parker, 2005a, 2005b, 2008). In posterior view, the two flanges exhibit a highly obtuse flexure ~180°, thus they are widely separated from each other allowing the lateral osteoderm to lay flat on a horizontal plane (Figure 7b,i), similar to the sacral lateral osteoderm (Figure 6h). They are unlike the acutely flexed anterior-caudal osteoderms observed in *T. coccinarum* (Heckert et al., 2010; Long & Murry, 1995; Martz, 2002) or the anterior-caudal lateral osteoderms observed in *D. spurensis* (Parker, 2008) which exhibit a 90° flexure. The dorsal eminence remains a moderately developed, posteriorly recurved spine; however, it is evident that it gradually reduces in prominence posteriorly down the caudal series. This gradual reduction of the eminence is well documented in *C. wellesi* (UMMP 13950; Case, 1932; Parker, 2018a), *D. spurensis* (MNA V9300; Parker, 2008), and *Paratypothorax* sp. (PEFO 3004, Hunt & Lucas, 1992; Lucas et al., 2006).

The external surface exhibits a well-incised radial ornamentation composed of elongated grooves radiating from the dorsal eminence (Figure 7f). On the dorsal flange, those grooves are continuations of the ornamentation on the adjacent paramedian osteoderm (Figure 7a). The anterior margin is no longer characterized as an ornamented area, instead the radial ornamentation extends to the anterior margin (Figure 7f). In the anterior-caudal region, the medial edge is strongly sigmoidal and matches the strongly sigmoidal lateral edge of the adjacent paramedian osteoderm (Figure 7a). The strong sigmoidal nature of the medial edge is unlike the weakly sigmoidal/straight medial edge observed in the anterior-trunk region of *Stenomyti huangae* (DMNH V.55054, DMNH V. 61392, Small & Martz, 2013), *C. wellesi* (UMMP 13950, Case, 1932; Parker, 2018a), *C. kahleorum* (NMMNH P-18496, Heckert & Lucas, 1999), *A. ferratus* (SMNS 5770, Schoch, 2007), *D. spurensis* (MNA V9300, Parker, 2008), and *Paratypothorax* sp. (PEFO 3004, Lucas et al., 2006). The sinuous nature of this margin produces an anteroposteriorly broad and medially projecting tongue-like process just posterior of the incision for the contact with the anterolateral process the adjacent paramedian osteoderm. A similar feature is present in the lateral osteoderms derived from the pelvic and/or anterior-caudal region of

R. chamaensis (NMMNH P-32797, P-32796, Lucas et al., 2006; Parker, 2007). However, in this taxon, the tongue-like process is highly reduced in comparison and the medial edge becomes anteroposteriorly straight directly posterior of it rather than remain sinuous. This suggests that the strong sigmoidal nature of the medial edge in TTU-P 10449 is an autapomorphy of *G. muelleri*. The medial surface (=ventral in articulation) of the lateral osteoderm is smooth and perforated by two foramina at the center of ossification.

5.3 | Ribs

TTU-P 10449 preserves several disarticulated ribs from both sides of the body that vary in preservation (Figure 9); some are fragmented while others are relatively complete. Comparison to other aetosaur taxa is limited because many of the reported individuals lack associated ribs or, if preserved, the ribs are often obscured from view as exemplified by the articulated specimens of *T. coccinarum* (NMMNH P-12964, P-56299, Heckert et al., 2010), *A. ferratus* (SMNS 5770, Schoch, 2007), and *C. kahleorum* (NMMNH P-18496, Heckert & Lucas, 1999). Currently, only *D. spurensis* (UMMP 7476, Case, 1922), *L. meadei* (TMM 31185-84, Sawin, 1947), and *T. coccinarum* (PEFO 42506; Parker et al., 2023) preserve sufficient rib material that can be compared with those of TTU-P 10449; however, only those of *D. spurensis* are formally described and figured (Case, 1922; Parker, 2008). The disparity in morphology (described below) indicates that the preserved ribs are derived from the cervical and trunk regions.

5.3.1 | Cervical and anterior-trunk regions

TTU-P 10449 preserves a robust, relatively complete trunk rib with an approximate length of 45 cm; the distal end of the rib is not preserved (Figure 9a). Proximally, the rib exhibits an "L"-shape. The capitulum, which articulates with the parapophysis on the corresponding

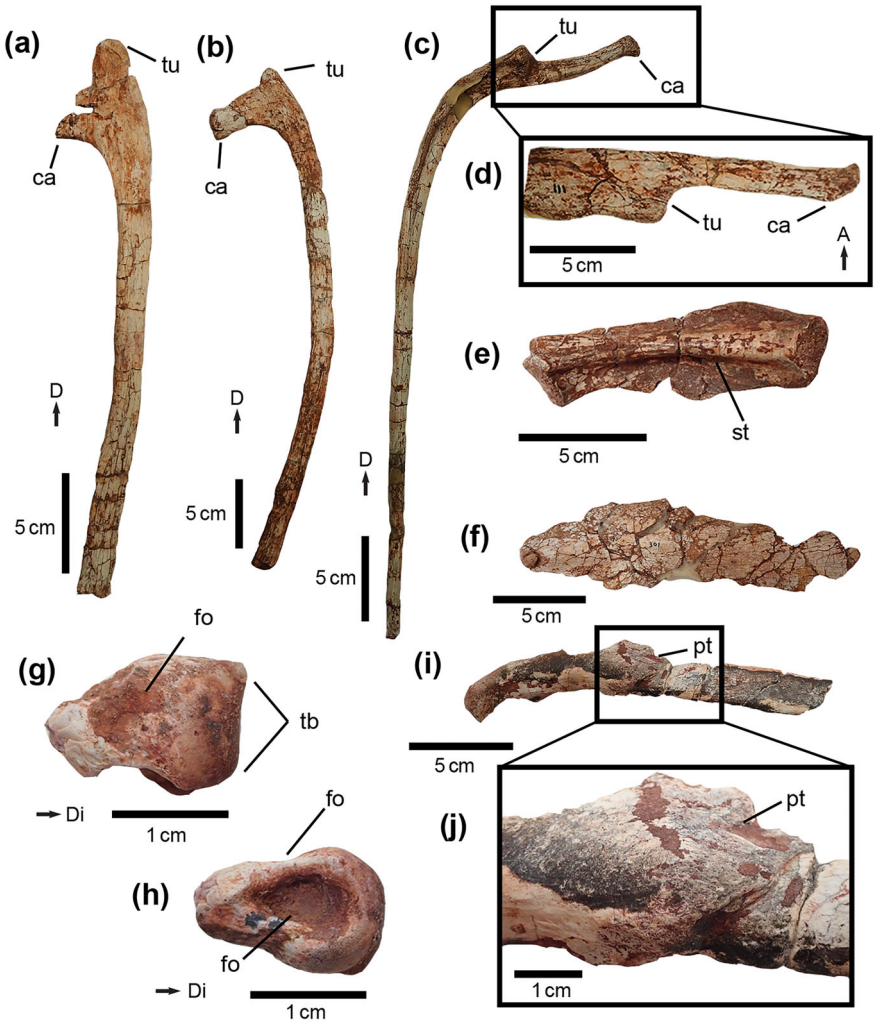

FIGURE 9 Ribs and podial in *Garzapelta muelleri* gen. et sp. nov. (TTU-P 10449). (a,b) Cervical and/or anterior-trunk ribs. (c,d) Mid-trunk rib with proximal end expanded in bounded box (d). (e,f,i,j) Trunk rib fragments. (i,j) Rib fragment with evidence of a healed fracture. (g,h) Distal end of phalanx. A, anterior; ca, capitulum; D, dorsal; Di, distal; fo, fossa; pt, pathology; st, strut; tb, tuber; tu, tuberculum. Orientations: Anterior/posterior: a,b; Posterior: c; Medial/lateral: f,h–j; Medial: e; Dorsal: d,g. Arrows indicate anatomical direction.

vertebra, is large, broad, transversely oriented with an ovate articulation surface (Figure 9a). On the other hand, the tuberculum, which articulates with the diapophysis on the corresponding vertebra, is characterized as a small protuberance and is located on the rib body (Figure 9a). In articulation, the shaft of the rib descends ventrally and gradually curves medially. The rib exhibits a ridge that originates at the tuberculum and runs the length of the shaft. The morphology of the proximal end indicates that this rib likely articulates to the first trunk vertebra, where the parapophysis has not transitioned from the centrum onto the transverse process of the neural arch; this morphology is best observed in *D. spurensis* (UMMP 7476, Case, 1922, figures 10 and 14, plate 7; MNA V9300, Parker, 2008, figure 7) which preserve a vertebral series that includes the cervical-to-trunk transition. Additionally, there are several rib fragments that exhibit a similar morphology to the rib described above; however, the proximal end is well-bifurcated; the tuberculum is broadly expanded and elongated with an ovate articulation surface, while the capitulum is more reduced and narrow in comparison (Figure 9b). This morphology aligns with that of ribs derived from the posterior cervical region (Walker, 1961, figure 11).

5.3.2 | Mid- and posterior-trunk regions

In the mid- and posterior-trunk regions, the parapophysis is located on the transverse process, just anterior of the diapophysis (e.g., *Stagonolepis robertsoni*, Walker, 1961; Desojo et al., 2013, figure 5); a condition that aetosaurs share with extant crocodyliforms (e.g., *A. mississippiensis*, Frey, 1988; *Alligator sinensis*, Cong et al., 1998). Accordingly, the capitulum is positioned anterior to and on the same transverse plane as the tuberculum on the ribs within these regions (Figure 9d). Thus, it is evident that TTU-P 10449 preserves several ribs that are derived from the mid-trunk region; the posterior-trunk region encompasses a smaller portion of the trunk in comparison. In articulation, ribs derived from the mid-trunk region exhibit a proximal end that is inclined ventrolaterally with a transversely elongate capitulum, while the tuberculum is positioned more distally on the rib body (Figure 9c). Both the capitulum and tuberculum exhibit an ovate articulation surface. There is no evidence of co-ossification between the proximal end of the rib with the transverse process of an adjacent vertebra; a condition described in *D. spurensis* (UMMP 7476, Case, 1922; MNA V9300, Parker, 2008), *S. deltatylus* (PEFO 34045, Parker, 2016b), and *C. wellesi* (UMMP 13950, Case, 1932; Parker, 2018a, Parker, 2018b). The rib body is anteroposteriorly expanded in the lateral view but exhibits a ventrally descending strut in medial view (Figure 9e); the bone is mediolaterally compressed and expands both anterior and posterior to the shaft. Additionally, the strut becomes confluent with the main rib shaft as it descends ventrally. The proximal half of the rib shaft bows laterally and then trends medially towards the distal end, which is ovate in cross-section (Figure 9c). The largest preserved mid-trunk rib in TTU-P 10449 exhibits a length of ~55 cm, but it is missing both the proximal and distal ends. Overall, the morphology described above is best exemplified by the mid-trunk ribs of *T. coccinarum* (PEFO 42506; Parker et al., 2023) and *S. deltatylus* (PEFO 34045, Parker, 2016b, figure 18d).

TTU-P 10449 preserves a rib fragment that is gracile and compressed with evidence of a weakly developed strut (Figure 9f); this indicates that the rib fragment is mediolaterally compressed distally, unlike the condition described in the mid-trunk ribs. Comparison to the trunk ribs of *D. spurensis* (MNA V9300, Parker, 2008), *C. wellesi* (UMMP 13950, Case, 1932; Parker, 2018a; PEFO 46222), and *T. coccinarum* (PEFO 42506, Parker et al., 2023) indicate that this morphology is characteristic of ribs derived from the posterior-trunk region; in that region the trunk ribs are gradually reduced in size with a rib shaft that is mediolaterally compressed including the distal end. Additionally, TTU-P 10449 preserves a rib fragment that shows evidence of a fracture that resulted in the displacement of the rib shaft (Figure 9i). The fracture shows evidence of uneven bone growth, thus indicating that the rib healed during life (Figure 9j).

5.4 | Podial

A partially preserved podial is the only representative of the appendicular region in TTU-P 10449. Only the distal end of this element is preserved (Figure 9g,h), so we are unable to discern if the element is a metacarpal, metatarsal, or phalanx. This fragment exhibits a morphology like the podials observed in *T. coccinarum* (MCZ 1488, Lucas & Heckert, 2011; NMMNH P-56299, P-12964, Heckert et al., 2010), *A. brasiliensis* (CPE2 168, Desojo et al., 2012), *Stagonolepis olenkae* (ZPAL AbIII/3349/1, Dróżdż, 2018), *Neoaetosauroides engaeus* (PVL 3525, Desojo & Báez, 2005), and *L. meadei* (TMM 31185-84, Sawin, 1947); it is spool-shaped, transversely broad, and dorsoventrally compressed with a shallow dorsoventrally oriented sulcus on the articulation surface separating the two tubers (Figure 9g). Additionally, there are deep, elliptical fossae on both the medial and lateral surfaces of the distal end, and a shallow fossa on its dorsal surface (Figure 9g,h); these fossae mark the insertion points of associated tendons and ligaments as observed in extant crocodylians (Meers, 2003).

5.5 | Phylogenetic analysis

Garzapelta muelleri gen. et sp. nov. was incorporated into the most recent matrix of the Aetosauria presented by Haldar et al. (2023) and analyzed via parsimony and Bayesian inference using four iterations of the matrix (see Section 3). Iteration two (Figure 10b,d), which included only lateral osteroderms of *G. muelleri*, and iteration three (Figure 11a,c), which included all osteoderms of that taxon, both recovered *G. muelleri* within the Stagonolepidoidea as a sister taxon to the Desmatosuchini in both parsimony (Figures 10b and 11a) and Bayesian analyses (Figures 10d and 11c). Additionally, the topologies are nearly identical between both iterations; however, *L. meadei* and *L. hunti* switch topological positions between the Bayesian consensus trees of iterations two (Figure 10d) and three (Figure 11c).

The resolution of the cladograms varies between the parsimony (Figures 10b and 11a) and Bayesian consensus trees (Figures 10d and 11c); the parsimony analyses recovered a large polytomy near the base of the Aetosauria at the node for the Stagonolepididae, while the Bayesian consensus trees are fully resolved. Interestingly, unlike iterations two and three, iteration one (Figure 10a,c), which

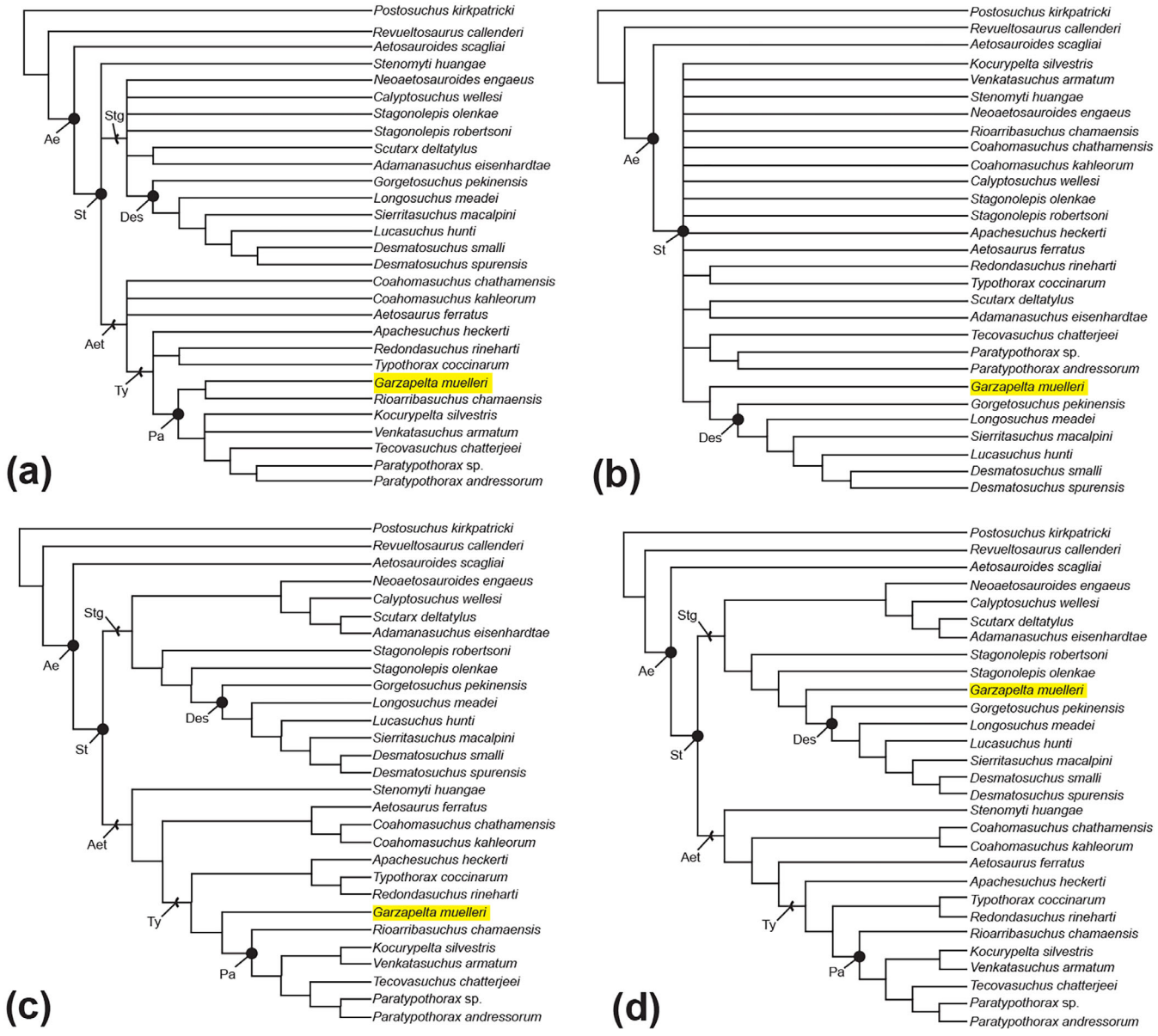

FIGURE 10 Phylogenetic analysis of the Aetosauria. (a,c) Iteration one, scoring only paramedian osteoderms of *Garzapelta muelleri* gen. et sp. nov. (TTU-P 10449). (b,d) Iteration two, scoring only lateral osteoderms of *Garzapelta muelleri*. (a,b) parsimony strict consensus and (c,d) Bayesian consensus trees. The topological position of *Garzapelta muelleri* is indicated by the yellow highlight. Ae, Aetosauria; Aet, Aetosaurinae; Des, Desmatosuchini; Pa, Paratypothoracini; St, Stagonolepididae; Stg, Stagonolepidoidea; Ty, Typothoracinae.

includes only paramedian osteoderms of *G. muelleri*, recovered *G. muelleri* within the Aetosaurinae in both the parsimony and Bayesian consensus trees. However, *G. muelleri* varies in its topological position across both cladograms. In the parsimony analysis (Figure 10a), *G. muelleri* is recovered within the Paratypothoracini as a sister taxon of *R. chamaensis*. On the other hand, in the Bayesian analysis (Figure 10c) *G. muelleri* is recovered directly basal to *R. chamaensis* as a sister taxon to the Paratypothoracini. The topologies across the parsimony and Bayesian consensus trees of iteration one are similar, albeit with a different degree of resolution. The two major aetosaurian clades, Stagonolepidoidea and Aetosaurinae, are evident in the strict consensus tree (Figure 10a); however, they are in a polytomy alongside *Stenomyti huangae*. The variation in the topological position of *G. muelleri* across these three iterations (Figures 10 and 11a,c) of the matrix indicates a discordance in the phylogenetic signal of the dorsal carapace in TTU-P 10449.

When scoring all osteoderms of TTU-P 10449 (Figure 11a,c; iteration three), the strict consensus (Figure 11a) recovered a larger polytomy than one

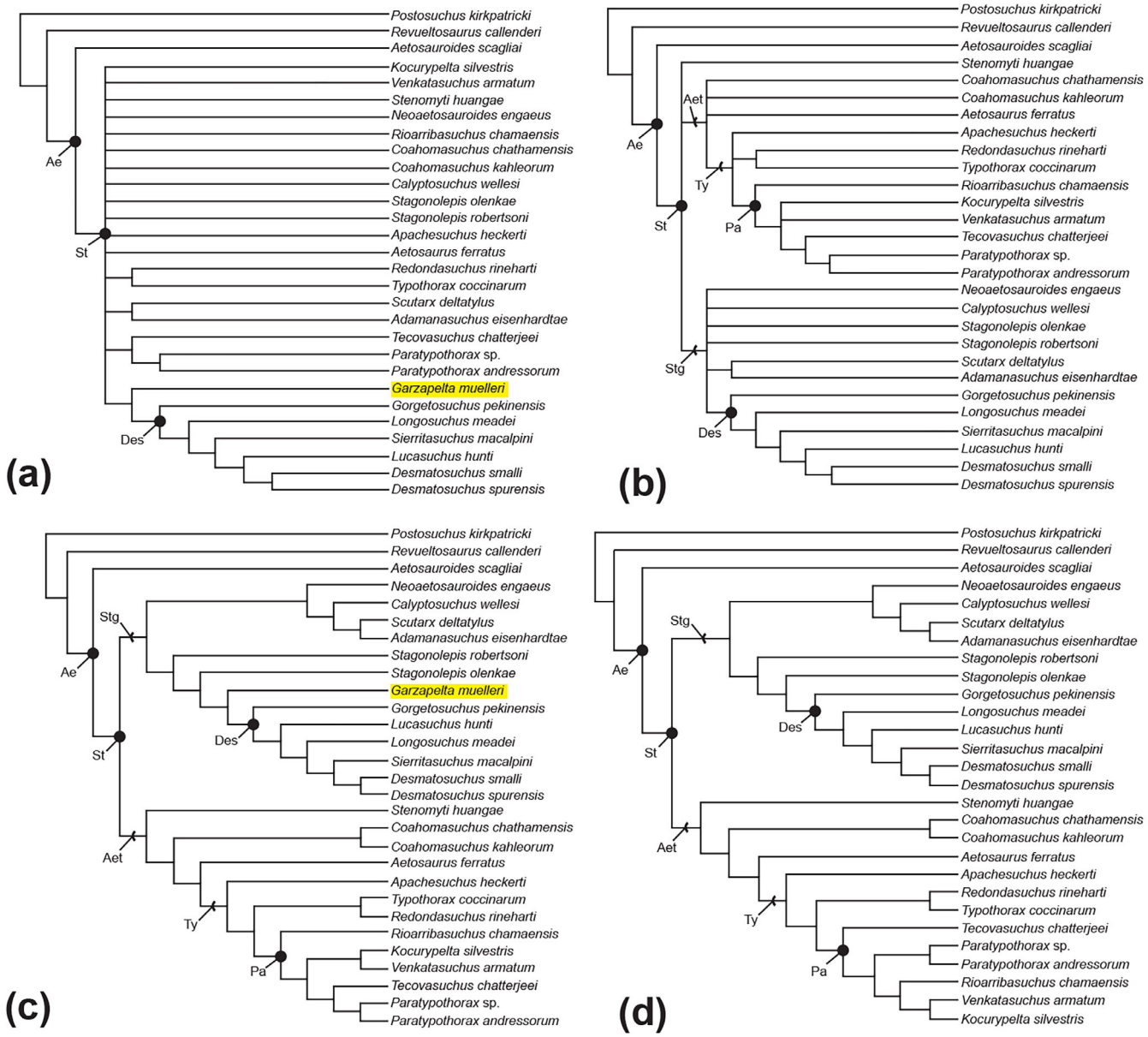

FIGURE 11 Phylogenetic analysis of the Aetosauria. (a,c) Iteration three, scoring all osteoderms of *Garzapelta muelleri* gen. et sp. nov. (TTU-P 10449). (b,d) Iteration four omitting *G. muelleri*. (a,b) parsimony strict consensus and (c,d) Bayesian consensus trees. The topological position of *G. muelleri* is indicated by the yellow highlight. Ae, Aetosauria; Aet, Aetosaurinae; Des, Desmatosuchini; Pa, Paratypothoracini; St, Stagonolepididae; Stg, Stagonolepidoidea; Ty, Typothoracinae.

presented by Haldar et al. (2023). The main similarity is the nested clade Desmatosuchini, which is recovered across this study (Haldar et al., 2023; Paes-Neto et al., 2021b; Parker, 2016a; Reyes et al., 2020). On the other hand, the Bayesian consensus tree (Figure 11c) is most similar to the strict consensus tree presented by Parker (2016a) and Reyes et al. (2020), particularly in the topological positions of *S. robertsoni*, *S. olenkae*, and *N. engaeus*. In the Baysian consensus tree, both species of *Stagonolepis* are recovered basal to the Desmatosuchini similar to *G. muelleri*. In comparison, *N. engaeus* is recovered in a clade where it is basal to *C. wellesi*, *S. deltatylus*, and *A. eisenhardtae*. Interestingly, when we omit *G. muelleri* from the analyzes (Figure 11b,d; iteration four) the strict consensus and Bayesian consensus trees resemble the topologies of iteration one (Figure 10a,c; only paramedian osteoderms scored for *G. muelleri*), rather than those of iteration three (Figure 11a,c; all osteoderms scored for *G. muelleri*), respectively. In iteration four, both *Stagonolepis* species and *Neoaetosauroides* are recovered in a polytomy at the base of the Stagonolepidoidea in the parsimony analysis (Figure 11b). However, in the Bayesian consensus tree (Figure 11d) their topological positions remain unchanged from the Bayesian consensus tree of iteration three (Figure 11c).

6 | DISCUSSION

6.1 | Phylogenetic implications

Since the original discovery of TTU-P 10449, the taxonomic affinities of *G. muelleri* have been contentious. This is because the preserved dorsal carapace of TTU-P 10449 (Figure 12) shows a degree of similarity to both the paratypothoracin *R. chamaensis* and the desmatosuchin *Desmatosuchus* (Martz, 2008; Martz et al., 2003); where the paramedian osteoderms resemble those of the former and the lateral osteoderms resemble those of the latter, bringing to question whether *G. muelleri* is a paratypothoracin aetosaur that exhibits convergent morphologies with desmatosuchins or vice-versa.

Because of the discordance in our qualitative assessment of TTU-P 10449, we decided to assess the taxonomic relationships of *G. muelleri* quantitatively through several phylogenetic analyses. However, our phylogenetic results indicate that the paramedian and lateral osteoderms of the preserved carapace of TTU-P 10449 provide conflicting phylogenetic signals (Figure 10). When only scoring the lateral osteoderms of TTU-P 10449 (Figure 10b,d; iteration two), *G. muelleri* is recovered as a sister taxon of the Desmatosuchini, directly basal to *G. pekinensis*; this

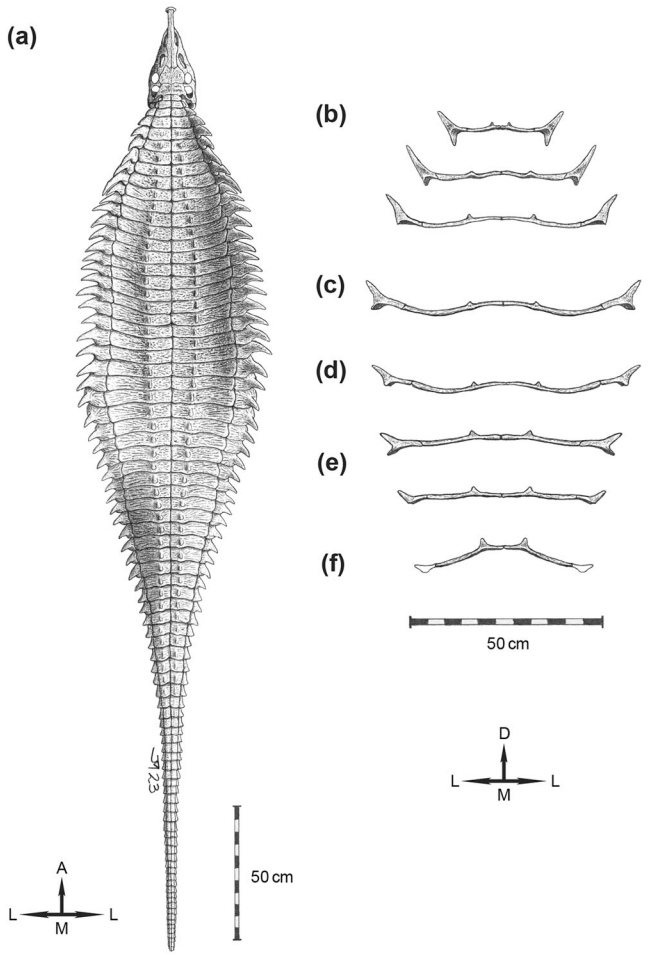

FIGURE 12 Hypothetical reconstruction of *Garzapelta muelleri* gen. et sp. nov. based on TTU-P 10449. (a) Carapace in dorsal view and (b–f) cross-sections of the carapace in posterior view. Cross-sections of the (b) posterior-cervical and anterior-trunk, (c) mid-trunk, (d) posterior-trunk and sacral, (e) anterior-caudal, and (f) mid-caudal regions. Reconstructed illustration by coauthor Jeffrey Martz. A, anterior; D, dorsal; L, lateral; M, medial. Arrows indicate anatomical direction.

aligns with initial qualitative assessments. On the other hand, when only scoring the paramedian osteoderms of TTU-P 10449 (Figure 10a,c; iteration one), *G. muelleri* is recovered as a sister taxon of the Paratypothoracini via Bayesian inference (Figure 10c) or as a sister taxon of *R. chamaensis* within the Paratypothoracini via parsimony (Figure 10a); both these results align with initial qualitative assessments. The disagreement in these two phylogenetic analyses indicate that the dorsal osteoderms of *G. muelleri* are indeed convergent to some degree.

When scoring both paramedian and lateral osteoderms together (Figure 11a,c; iteration three), *G. muelleri* is recovered as a sister taxon of the Desmatosuchini, suggesting that *G. muelleri* is convergent with paratypothoracins, primarily *Rioarriabuschus chamaensis*. As

a result, this also suggests that the character combination associated with paratypothoracin paramedian osteoderms are plesiomorphic to the Stagonolepididea and have reversed in all reported taxa (~20 species) except paratypothoracins and *G. muelleri*. However, when considering the alternative hypothesis that *G. muelleri* is a paratypothoracin (Figure 10a,c), this suggests that the lateral osteoderms, particularly in the trunk region (Figures 5 and 6), are convergent with those of desmatosuchins in the shape of the dorsal eminence, and shape and proportional size of the dorsal flange. This is further supported by the style of articulation between the paramedian and lateral osteoderms of *G. muelleri*. An anteromedial corner of the lateral osteoderm that overlaps the anterolateral corner of the adjacent paramedian osteoderm, and a rigid articulation between these elements are defining synapomorphies of the Desmatosuchini (Parker, 2007); both states are absent in *G. muelleri* (Figures 4 and 8). Additionally, the wide obtuse flexure exhibited by the trunk lateral osteoderms of *G. muelleri* align with the plesiomorphic condition of the Stagonolepididae (Parker, 2016a; Parker, 2016b), unlike the derived condition of desmatosuchins, which exhibit a flexure of 90° (Parker, 2007; Parker & Martz, 2010), or those of derived paratypothoracins which are strongly acute (Haldar et al., 2023; Heckert et al., 2010; Lucas et al., 2006; Martz et al., 2013; Parker, 2007).

When considering both hypotheses, the most parsimonious explanation is that *G. muelleri* (Figure 12) is a paratypothoracin that is closely related to *R. chamaensis* with lateral osteoderms that are slightly convergent with those of desmatosuchins as seen in iteration one (Figure 10a,c) and as originally hypothesized by Martz et al. (2003). However, the fact that we do not recover *G. muelleri* as a close relative of *R. chamaensis* when scoring all osteoderms together (Figure 11a,c; iteration three) indicates that our current matrix and character lists are not fully accounting for the disparity in morphology of the aetosaurian dorsal carapace, particularly the degree of convergence. Thus, it is important to be cautious when including *G. muelleri* into a phylogenetic assessment as it can influence the topology of the Aetosauria and how we interpret the evolutionary relationships of these taxa (Figure 12).

6.2 | Implications on Rioarribasuchus and similar taxa

The description of *G. muelleri* (Figure 12) prompted several revised interpretations of *Rioarribasuchs chamaensis*, which is primarily known from several disarticulated osteoderms. Parker (2007) originally scored *R. chamaensis* as exhibiting trunk paramedian osteoderms with a W:L of 3.5 or greater (character 14-1, Parker, 2007; character 64-2, Parker, 2016a, Parker, 2016b). However, several trunk paramedians of *R. chamaensis* (i.e., NMMNH P-34887, 33820, 35807) exhibit a W:L between 3.0 and 3.5 (character 64-1, see Supporting information S1 and S2). Additionally, the trunk paramedian osteoderms of *R. chamaensis* were scored as exhibiting a "cutoff" corner on the posterolateral edge (character 63-1, Parker, 2016a, 2016b) similar to *A. eisenhardtae* (PEFO 34638, Lucas et al., 2007), *Paratypothorax* (PEFO 3004, Lucas et al., 2006; TTU-P 9169, Martz et al., 2013), and *T. chatterjeei* (TTU-P 545, Martz & Small, 2006). However, when comparing homologous elements across these taxa, the trunk paramedian osteoderms of *R. chamaensis* do not exhibit the distinctive angled incision that characterize these paramedian osteoderms. In accordance with this interpretation, we rescored *R. chamaensis* as exhibiting character state 63-0 in our study. Interestingly, the spines of the fragmentary lateral osteoderms (i.e., NMMNH P-35993, 32794; Parker, 2007) hypothesized to be derived from the trunk region of *R. chamaensis* bear a striking resemblance to the cervical lateral osteoderms of *G. muelleri* (Figure 4). Unfortunately, the dorsal and lateral flanges of NMMNH P-35993 and NMMNH P-32794 are not well preserved, which makes it unclear if these osteoderms were derived from the cervical region instead of the trunk.

Morphological understanding of *R. chamaensis* is relevant because there is documentation of a paratypothoracin, which has been tentatively identified as cf. *Rioarribasuchus*, from the Eagle Basin in northwestern Colorado (Martz and Small, 2019) with osteoderms that resemble those of both *R. chamaensis* and *G. muelleri*; where the lateral osteoderms resemble those of the former and the paramedian osteoderms resemble those of the latter. However, in order to assess the taxonomic affinities of this new material from the Eagle Basin requires a comprehensive understanding of the anatomy and phylogenetic relationships of both *R. chamaensis* and *G. muelleri*.

7 | CONCLUDING REMARKS

The discovery of *G. muelleri* gen. et sp. nov., from MOTT 3882 (the UU Sand Creek locality), within the Late Triassic middle unit of the Cooper Canyon Formation (latest Adamanian or earliest Revueltian estimated holochronozone; Dockum Group) in Texas provides new insight into the interspecific variation of the dorsal carapace within

the Aetosauria. It is evident that the morphology of the lateral osteoderms is driving the final topological position of *G. muelleri*, recovering it as a sister taxon of the Desmatosuchini. However, we hypothesize that *G. muelleri* is a paratypothoracin aetosaur with lateral osteoderms that are convergent with those of desmatosuchins, as this is the most parsimonious explanation for assessing the homoplasticity within the Aetosauria. *G. muelleri* highlights the limitations of our current matrix and character lists as it exhibits a degree of convergence that our current analyses cannot resolve; it indicates that we are not fully accounting for the morphological disparity within the aetosaurian carapace, particularly its convergence across taxa. Thus, including *G. muelleri* into a phylogenetic analysis merits caution as it can result in a nonparsimonious topology that can have severe impacts on our interpretations of the relationships within the Aetosauria. Additionally, this new taxon brings to question our current anatomical and phylogenetic understanding of *R. chamaensis*. However, the similarities between *G. muelleri*, *R. chamaensis*, and the paratypothoracin from the Eagle Basin in Colorado do suggest that we are likely dealing with the emergence of a new group of aetosaur that exhibits a biostratigraphical range that is likely confined to the Revueltian estimated holochronozone (middle to late Norian, 215–207 Ma, Martz & Parker, 2017) but may be as old as latest Adamanian.

AUTHOR CONTRIBUTIONS

William A. Reyes: Conceptualization; investigation; writing—original draft; writing – review and editing; visualization; formal analysis; software; project administration; supervision; validation; methodology; funding acquisition. **Jeffrey Martz:** Conceptualization; investigation; visualization; writing—review and editing; resources; data curation; writing—original draft; validation. **Bryan J. Small:** Resources; conceptualization; investigation; writing—review and editing; data curation; visualization; writing—original draft; validation; funding acquisition.

ACKNOWLEDGMENTS

The authors thank Kendra Dean and John-Henry Voss from TTU-P for providing collection history and access to and assistance with the holotype specimen of *G. muelleri*. Excavation work was led by Bill Mueller and assisted by Emmett Shedd. Thank you to ranch owner Kenneth Marts for permitting the excavation of the MOTT 3882 locality within their property. Preparation of the specimen was done by Bill Mueller. Christopher Bell provided constructive feedback in the development of the article. We thank the editor Felipe Pinheiro, William Parker, and an anonymous reviewer for their constructive reviews which helped strengthen this article. Partial financial support was provided by the estates of Kristen Waller and Sun Youli (to B. J. Small). Additionally, this study was partially funded by the National Science Foundation (Grant No. 2137420) and Endowed Presidential Scholarship, Jackson School of Geosciences, The University of Texas at Austin (to W. A. Reyes). Any opinions, findings, and conclusions or recommendations expressed in this material are those of the authors and do not necessarily reflect the views of the National Science Foundation.

ORCID

William A. Reyes https://orcid.org/0000-0002-9967-2557
Jeffrey W. Martz https://orcid.org/0000-0003-1398-2528
Bryan J. Small https://orcid.org/0009-0004-6924-4924

REFERENCES

Atannasov, M. N. (2002). *Two new archosaur reptiles from the Late Triassic of Texas*. [PhD Dissertation]. Texas Tech University, Lubbock, Texas. 352 p.

Atchley, S. C., Nordt, L. C., Dworkin, S. I., Ramezani, J., Parker, W. G., Ash, S. R., & Bowring, S. A. (2013). A linkage among pangean tectonism, cyclic alluviation, climate change, and biological turnover in the Late Triassic: The record from the Chinle formation, southwestern United States. *Journal of Sedimentary Research*, *83*, 1147–1161.

Biacchi Brust, A. C., Desojo, J. B., Schultz, C. L., Paes-Neto, V. D., & Da-Rosa, Á. A. S. (2018). Osteology of the first skull of *Aetosauroides scagliai* Casmiquela 1960 (Archosauria: Aetosauria) from the Upper Triassic of southern Brazil (*Hyperodapedon* assemblage zone) and its phylogenetic importance. *PLoS One*, *13*, e0201450.

Casamiquela, R. M. (1961). Dos nuevos estagonolepoideos Argentinos (de Ischigualasto, San Juan). *Revista de la Asociación Geológica Argentina*, *16*, 143–203.

Case, E. C. (1920). Preliminary description of a new suborder of phytosaurian reptiles with a description of a new species of *Phytosaurus*. *Journal of Geology*, *28*, 524–535.

Case, E. C. (1922). *New reptiles and stegocephalians from the Upper Triassic of western* (Vol. 321, pp. 1–84). Carnegie Institution of Washington Publication.

Case, E. C. (1932). *A perfectly preserved segment of the armor of a phytosaur, with associated vertebrae: Contributions from the museum of paleontology* (Vol. 4, pp. 57–80). University of Michigan.

Cong, L., Hou, L., Wu, X. C., & Hou, J. F. (1998). *[Chinese] 扬子鳄大体解剖. [English] the gross anatomy of Alligator sinensis Fauvel*. China Science and Technology Press.

Cope, E. D. (1869). Synopsis of extinct Batrachia, Reptilia, and Aves of North America. *Proceedings of the Academy of National Sciences Philadelphia*, *1868*, 208–221.

Cope, E. D. (1875). Report on the geology of that part of New Mexico examined during the field season of 1874, in Wheeler, G.M., ed., Annual report upon the geographical explorations west of the one hundredth meridian in California, Nevada,

Nebraska, Utah, Arizona, Colorado, New Mexico, Wyoming and Montana: Washington, DC: United States Government Printing Office, (61–97 of separate report LL).

Czepiński, Ł., Dróżdż, D., Szcygielski, T., Tałanda, M., Pawlak, W., Lewczuk, A., Rytel, A., & Sulej, T. (2021). An Upper Triassic terrestrial vertebrate assemblage from the forgotten Kocury locality (Poland) with a new aetosaur taxon. *Journal of Vertebrate Paleontology*, *41*, e1898977.

Desojo, J. B., & Báez, A. M. (2005). El esqueleto postcraneano de *Neoaetosauroides* (Archosauria: Aetosauria) del Triásico Superior del centro-oeste de Argentina. *Ameghiniana*, *42*, 115–126.

Desojo, J. B., & Ezcurra, M. D. (2011). A reappraisal of the taxonomic status of *Aetosauroides* (Archosauria, Aetosauria) specimens from the Late Triassic of South America and their proposed synonymy with *Stagonolepis*. *Journal of Vertebrate Paleontology*, *31*, 596–609.

Desojo, J. B., Ezcurra, M. D., & Kischlat, E. E. (2012). A new aetosaur genus (Archosauria: Pseudosuchia) from the early Late Triassic of southern Brazil. *Zootaxa*, *3166*, 1–33.

Desojo, J. B., Heckert, A. B., Martz, J. W., Parker, W. G., Schoch, R. S., Small, B. J., & Sulej, T. (2013). Aetosauria: A clade of armoured pseudosuchians from the Upper Triassic continental beds. In S. J. Nesbitt, J. B. Desojo, & R. B. Irmis (Eds.), *Anatomy, phylogeny, and Palaeobiology of early archosaurs and their kin: Geological society* (Vol. 379, pp. 203–239). Special Publications.

Desojo, J. B., & Vizcaíno, S. F. (2009). Jaw biomechanics in the south American aetosaur *Neoaetosauroides engaeus*. *Paläontologische Zeitschrift*, *83*, 499–510.

Dróżdż, D. (2018). Osteology of a forelimb of an aetosaur *Stagonolepis olenkae* (Archosauria: Pseudosuchia: Aetosauria) from the Krasiejów locality in Poland and its probable adaptations for a scratch-digging behavior. *PeerJ*, *6*, e5595.

Dunlavey, M. G., Whiteside, J. H., & Irmis, R. B. (2009). Ecosystem instability during the rise of the dinosaurs: Evidence from the Late Triassic in New Mexico and Arizona. *Geological Society of America Abstracts with Programs*, *41*, 477.

Ezcurra, M. D. (2016). The phylogenetic relationships of basal archosauromorphs, with an emphasis on the systematics of proterosuchian archosauriforms. *PeerJ*, *4*, e1778.

Fitch, A. J., Haas, M., C'Hair, W., Ridgley, B., Oldman, D., Reynolds, C., & Lovalace, D. M. (2023). A new rhyncosaur taxon from the Popo Agie formation, WY: Implications for a northern Pangean early-Late Triassic (Carnian) Fauna. *Diversity*, *15*, 544.

Frey, E. (1988). Anatomie des körperstammes von *Alligator mississippiensis* Daudin. *Stuttgart Beiträge zur Naturkunde Serie A*, *424*, 1–106.

Gauthier, J., & Padian, K. (1985). Phylogenetic, functional, and aerodynamic analyses of the origin of birds and their flight. In M. K. Hecht, J. H. Ostrom, G. Viohl, & P. Wellnhofer (Eds.), *The beginning of birds: Proceedings of the international archaeopteryx conference* (pp. 185–197). Freunde des Jura Museums.

Goloboff, P. A., Farris, J. S., & Nixon, K. C. (2008). TNT, a free program for phylogenetic analysis. *Cladistics*, *24*, 774–786.

Haldar, A., Ray, S., & Bandyopadhyay, S. (2023). A new typothoracine aetosaur (Archosaur: Pseudosuchia) from the Upper Triassic of India with insights on biostratigraphy, diversity, and paleobiogeography. *Journal of Vertebrate Paleontology*, *43*, e2253292.

Heckert, A. B., Fraser, N. C., & Schneider, V. P. (2017). A new species of *Coahomasuchus* (Archosauria, Aetosauria) from the Upper Triassic Pekin formation, Deep River Basin, North Carolina. *Journal of Paleontology*, *91*, 162–178.

Heckert, A. B., & Lucas, S. G. (1999). A new aetosaur (Reptilia: Archosauria) from the Upper Triassic of Texas and the phylogeny of aetosaurs. *Journal of Vertebrate Paleontology*, *19*, 50–68.

Heckert, A. B., & Lucas, S. G. (2000). Taxonomy, phylogeny, biostratigraphy, biochronology, paleobiogeography, and evolution of the Late Triassic Aetosauria (Archosauria: Crurotarsi). *Zentralblatt für Gelogie und Paläontologie*, *1*, 1539–1587.

Heckert, A. B., & Lucas, S. G. (2002). South American occurrences of the Adamanian (Late Triassic: Latest Carnian) index taxon *Stagonolepis* (Archosauria: Aetosauria) and their biochronological significance. *Journal of Paleontology*, *76*, 852–863.

Heckert, A. B., Lucas, S. G., Rinehart, L. F., Celeskey, M. D., Spielmann, J. A., & Hunt, A. P. (2010). Articulated skeletons of the aetosaur *Typothorax coccinarum* Cope (Archosauria: Stagnolepididae) from the Upper Triassic bull canyon formation (Revueltian: Early-mid Norian), eastern New Mexico. *USA: Journal of Vertebrate Paleontology, v.*, *30*, 619–642.

Heckert, A. B., Schneider, V. P., Fraser, N. C., & Webb, R. A. (2015). A new aetosaur (Archosauria, Suchia) from the Upper Triassic Pekin formation, Deep River basin, North Carolina, U.S.A., and its implications for early aetosaur evolution. *Journal of Vertebrate Paleontology*, *35*, e881831.

Hoffman, D. K., Heckert, A. B., & Zanno, L. E. (2019). Under the armor: X-ray computed tomographic reconstruction of the internal skeleton of *Coahomasuchus chathamensis* (Archosauria: Aetosauria) from the Upper Triassic of North Carolina, USA, and a Phylogenetic Analysis of Aetosauria. *PeerJ*, *6*, e4368.

Huelsenbeck, J. P., & Ronquist, F. (2001). MRBAYES: Bayesian inference of phylogeny. *Bioinformatics*, *17*, 754–755.

Hungerbühler, A., Mueller, B., Chatterjee, S., & Cunningham, D. P. (2013). Cranial anatomy of the Late Triassic phytosaur *Machaeroprosopus*, with the description of a new species from West Texas. *Earth and Environmental Science Transactions of the Royal Society of Edinburgh*, *103*, 269–312.

Hunt, A. P., & Lucas, S. G. (1992). The first occurrence of the aetosaur *Paratypothorax andressi* (Reptilia, Aetosauria) in the western United States and its biochronological significance. *Paläontologische Zeitschrift*, *66*, 147–157.

Lehman, T. M., & Chatterjee, S. (2005). Depositional setting and vertebrate biostratigraphy of the Triassic Dockum Group of Texas. *Journal of Earth System Science*, *114*, 325–351.

Lehman, T. M., Chatterjee, S., & Schnable, J. P. (1992). The Cooper Canyon Formation (Late Triassic) of western Texas. *Texas Journal of Science*, *44*, 349–355.

Lessner, E. J., Parker, W. G., Marsh, A. D., Nesbitt, S. J., Irmis, R. B., & Mueller, B. D. (2018). New insights into the Late Triassic dinosauromorph-bearing assemblages from Texas using apomorphy-based identifications. *PaleoBios*, *35*, 1–41.

Long, R. A., & Ballew, K. L. (1985). Aetosaur dermal armor from the Late Triassic of southwestern North America, with special reference to material from the Chinle formation of petrified Forest National Park. In E. H. Colbert & R. R. Johnson (Eds.),

The Petrified Forest Through the Ages, 75th Anniversary Symposium November 7, 1981 (Vol. *54*, pp. 45–68). Museum of Northern Arizona Bulletin.

Long, R. A., & Murry, P. A. (1995). Late Triassic (Carnian and Norian) tetrapods from the southwestern United States. *New Mexico Museum of Natural History and Science Bulletin*, *4*, 99–108.

Lovelace, D. M., Fitch, A. J., Schwartz, D., & Schmitz, M. (2023). *Concurrence of Late Triassic lithostratigraphic, radioisotopic, and biostratigraphy data support Carnian age for the Popo Agie formation (Chugwater group)*. GSA Bulletin. https://doi.org/10.1130/B36807.1

Lucas, S. G. (1993). The Chinle group: Revised stratigraphy and biochronology of Upper Triassic nonmarine strata in the western United States, in Morales, M., ed., Aspects of Mesozoic Geology and Paleontology of the Colorado Plateau. *Museum of Northern Arizona Bulletin*, *59*, 27–50.

Lucas, S. G. (1998). Global Triassic tetrapod biostratigraphy and biochronology. *Palaeogeography, Palaeoclimatology, Palaeoecology*, *143*, 347–384.

Lucas, S. G., & Heckert, A. B. (2011). Late Triassic aetosaurs as the trackmaker of the tetrapod footprint ichnotaxon *Brachychirotherium*. *Ichnos*, *18*, 197–208.

Lucas, S. G., Heckert, A. B., & Rinehart, L. F. (2006). The Late Triassic aetosaur *Paratypothorax*. *New Mexico Museum of Natural History and Science Bulletin*, *37*, 575–580.

Lucas, S. G., Hunt, A. P., & Spielmann, J. A. (2007). A new aetosaur from the Upper Triassic (Adamanian: Carnian) of Arizona. *New Mexico Museum of Natural History and Science Bulletin*, *40*, 241–247.

Lydekker, R. (1887). The Fossil Vertebrata of India. *Records of the Geological Society of India*, *20*, 51–80.

Maddison, W. P., & Maddison, D. R. (2023). Mesquite: A modular system for evolutionary analysis. Version 3.81. http://www.mesquiteproject.org

Marsh, A. D., Smith, M. E., Parker, W. G., Irmis, R. B., & Kligman, B. T. (2020). Skeletal anatomy of *Acaenasuchus geoffreyi* Long and Murry, 1995 (Archosauria: Pseudosuchia) and its implications for the origin of the aetosaurian carapace. *Journal of Vertebrate Paleontology*, *40*, e1794885.

Marsh, O. C. (1884). The classification and affinities of dinosaurian reptiles. *Nature*, *31*, 68–69.

Martz, J. W. (2002). *The Morphology and Ontogeny of Typothorax coccinarum (Archosauria, Stagonolepididae) from the Upper Triassic of the American Southwest*. [MS Thesis]. Department of Geoscience, Texas Tech University, Lubbock, Texas, 279 p.

Martz, J. W. (2008). *Lithostratigraphy, Chemostratigraphy, and Vertebrate Biostratigraphy of the Dockum Group (Upper Triassic), of Southern Garza County, West Texas*. [PhD Dissertation]. Texas Tech University, Lubbock, Texas. 504 p.

Martz, J. W., Kirkland, J. I., Milner, A. R. C., Parker, W. G., & Santucci, V. L. (2017). Upper Triassic lithostratigraphy, depositional systems, and vertebrate paleontology across southern Utah. *Geology of the Intermountain West*, *4*, 99–180.

Martz, J. W., Mueller, B., Nesbitt, S. J., Stocker, M. R., Parker, W. G., Atanassov, M., Fraser, N., Weinbaum, J., & Lehane, J. R. (2013). A taxonomic and biostratigraphic re-evaluation of the post quarry vertebrate assemblage from the Cooper canyon formation (Dockum Group, Upper Triassic) of southern Garza County, western Texas. *Earth and Environmental Science Transactions of the Royal Society of Edinburgh*, *103*, 339–364.

Martz, J. W., Mueller, B., & Small, B. J. (2003). Two new aetosaurs (Archosauria, Stagonolepididae) from the Upper Triassic of Texas and Colorado, and problems in aetosaur identification and taxonomy. *Journal of Vertebrate Paleontology*, *23*(3 Suppl), 76A.

Martz, J. W., & Parker, W. G. (2017). Revised formulation of the Late Triassic land vertebrate "faunachrons" of Western North America: Recommendations of codifying nascent systems of vertebrate biochronology. In W. G. Parker & K. E. Zeigler (Eds.), *Terrestrial depositional systems: deciphering complexities through multiple stratigraphic methods*. (pp. 39–125). Elsevier.

Martz, J. W., Parker, W. G., Skinner, L., Raucci, J. J., Umhoefer, P., & Blakey, R. C. (2012). *Geologic map of petrified Forest National Park* (p. 18). Arizona Geological Survey.

Martz, J. W., & Small, B. J. (2006). *Tecovasuchus chatterjeei*, a new aetosaur (Archosauria: Stagonolepididae) from the Tecovas formation (Carnian, Upper Triassic) of Texas. *Journal of Vertebrate Paleontology*, *26*, 308–320.

Martz, J. W., & Small, B. J. (2019). Non-dinosaurian dinosauromorphs from the Chinle Formation (Upper Triassic) of the Eagle Basin, northern Colorado: Dromomeron romeri (Lagerpetidae) and a new taxon, Kwanasaurus williamparkeri (Silesauridae). *PeerJ*, *7*, e7551.

Meers, M. B. (2003). Crocodylian forelimb musculature and its relevance to Archosauria. *The Anatomical Record*, *274A*, 891–916.

Mueller, B. D., Small, B. J., Jenkins, X., Huttenlocker, A. K., & Chatterjee, S. (2023). Cranial anatomy of *Libognathus sheddi* Small, 1997 (Parareptilia, Procolophonidae) from the Upper Triassic Dockum Group of West Texas, USA. *The Anatomical Record*, 1–21. https://doi.org/10.1002/ar.25364

Paes-Neto, V. D., Desojo, J. B., Brust, A. C. B., Ribeiro, A. M., Schultz, C. L., & Soares, M. B. (2021a). Skull osteology of *Aetosauroides scagliai* Casamiquela, 1960 (Archosauria: Aetosauria) from the Late Triassic of Brazil: New insights into the paleobiology of aetosaurs. *Palaeontologia Electronica*, *24*, a33. https://doi.org/10.26879/1120

Paes-Neto, V. D., Desojo, J. B., Brust, A. C. B., Ribeiro, A. M., Schultz, C. L., & Soares, M. B. (2021b). The first braincase of the basal aetosaur *Aetosauroides scagliai* (Archosauria: Pseudosuchia) from the Upper Triassic of Brazil. *Journal of Vertebrate Paleontology*, *41*, e1928681.

Paes-Neto, V. D., Desojo, J. B., Brust, A. C. B., Schultz, C. L., Da-Rosa, Á. A. S., & Soares, M. B. (2021c). Intraspecific variation in the axial skeleton of *Aetosauroides scagliai* (Archosauria: Aetosauria) and its implications for the aetosaur diversity of the Late Triassic of Brazil. *Annals of the Brazilian Academy of Sciences*, *93*, e20201239.

Parker, W. G. (2005a). A new species of the Late Triassic aetosaur *Desmatosuchus* (Archosauria: Pseudosuchia). *Comptes Rendus Palevol*, *4*, 327–340.

Parker, W. G. (2005b). Faunal review of the Upper Triassic Chinle formation of Arizona. *Mesa Southwest Museum Bulletin*, *11*, 34–54.

Parker, W. G. (2007). Reassessment of the aetosaur *'Desmatosuchus' chamaensis* with a reanalysis of the phylogeny of the Aetosauria (Archosauria: Pseudosuchia). *Journal of Systematic Palaeontology*, *5*, 41–68.

Parker, W. G. (2008). Description of new material of the aetosaur *Desmatosuchus spurensis* (Archosauria: Suchia) from the Chinle formation of Arizona and a revision of the genus *Desmatosuchus*. *PaleoBios*, *28*, 1–40.

Parker, W. G. (2016a). Revised phylogenetic analysis of the Aetosauria (Archosauria: Pseudosuchia): Assessing the effects of incongruent morphological character sets. *PeerJ*, *4*, e1583.

Parker, W. G. (2016b). Osteology of the Late Triassic aetosaur *Scutarx deltatylus* (Archosauria: Pseudosuchia). *PeerJ*, *4*, e2411.

Parker, W. G. (2018a). Redescription of *Calyptosuchus* (*Stagonolepis*) *wellesi* (Archosauria: Pseudosuchia: Aetosauria) from the Late Triassic of the southwestern United States with a discussion of genera in vertebrate paleontology. *PeerJ*, *6*, e4291.

Parker, W. G. (2018b). Anatomical notes and discussion of the first described aetosaur *Stagonolepis robertsoni* (Archosauria: Suchia) from the Upper Triassic of Europe, and the use of plesiomorphies in aetosaur biochronology. *PeerJ*, *6*, e5455.

Parker, W. G., & Martz, J. W. (2010). Using positional homology in aetosaur (Archosauria: Pseudosuchia) osteoderms to evaluate the taxonomic status of *Lucasuchus hunti*. *Journal of Vertebrate Paleontology*, *30*, 1100–1108.

Parker, W. G., & Martz, J. W. (2011). The Late Triassic (Norian) Adamanian-Revueltian tetrapod faunal transition in the Chinle formation of petrified Forest National Park, Arizona, Late Triassic terrestrial biotas and the rise of the dinosaurs. *Earth and environmental science transactions of the Royal Society of Edinburgh*, *101*, 231–260. (for 2010).

Parker, W. G., Nesbitt, S. J., Irmis, R. B., Martz, J. W., Marsh, A. D., Brown, M. A., Stocker, M. R., & Werning, S. (2021). Osteology and relationship of *Revueltosaurus callenderi* (Archosauria: Suchia) from the Upper Triassic (Norian) Chinle formation of petrified Forest National Park, Arizona, United States. *The Anatomical Record*, *305*, 2353–2414. https://doi.org/10.1002/ar.24757

Parker, W. G., Reyes, W. A., & Marsh, A. D. (2023). Incongruent ontogenetic maturity indicators in a Late Triassic archosaur (Aetosauria: *Typothorax coccinarum*). *The Anatomical Record*, 1–17. https://doi.org/10.1002/ar.25343

Parker, W. G., Stocker, M. R., & Irmis, R. B. (2008). A new desmatosuchine aetosaur (Archosauria: Suchia) from the Upper Triassic Tecovas formation (Dockum Group) of Texas. *Journal of Vertebrate Paleontology*, *28*, 692–701.

Ramezani, J., Fastovsky, D. E., & Bowring, S. A. (2014). Revised chronostratigraphy of the lower Chinle formation strata in Arizona and New Mexico (USA): High-precision U-Pb geochronological constraints on the Late Triassic evolution of dinosaurs. *American Journal of Science*, *314*, 981–1008.

Ramezani, J., Hoke, G. D., Fastovsky, D. E., Bowring, S. A., Therrien, F., Dworkin, S. I., Atchley, S. C., & Nordt, L. C. (2011). High precision U-Pb geochronology of the Late Triassic Chinle formation, petrified Forest National Park (Arizona, USA): Temporal constraints on the early evolution of dinosaurs. *Geological Society of America*, *123*, 2142–2159.

Rasmussen, C., Mundil, R., Irmis, R. B., Geisler, D., Gehrels, G. E., Olsen, P. E., Kent, D. V., Lepre, C., Kinney, S. T., Geissman, J. W., & Parker, W. G. (2020). U-Pb zircon geochronology and depositional age models for the Upper Triassic Chinle formation (petrified Forest National Park, Arizona, USA): Implications for Late Triassic Paleoecological and Paleoenvironmental Change. *Geological Society of America Bulletin*, *133*, 539–558. https://doi.org/10.1130/B35485.1

Reyes, W. A., Parker, W. G., & Heckert, A. B. (2023). A new aetosaur (Archosauria: Pseudosuchia) from the Upper Blue Mesa Member (Adamanian: Early–mid Norian) of the Late Triassic Chinle formation, northern Arizona, USA, and a review of the paratypothoracin *Tecovasuchus* across the southwestern USA. *PaleoBios*, *40*, 1–15.

Reyes, W. A., Parker, W. G., & Marsh, A. D. (2020). Cranial anatomy and dentition of the aetosaur *Typothorax coccinarum* (Archosauria: Pseudosuchia) from the Upper Triassic (Revueltian–mid Norian) Chinle formation of Arizona. *Journal of Vertebrate Paleontology*, *40*, e1876080.

Roberto-Da-Silva, L., Desojo, J. B., Cabreira, S. F., Aires, A. S. S., Müller, R. T., Pacheco, C. P., & Dias-Da-Silva, S. (2014). A new aetosaur from the Upper Triassic of the Santa Maria Formation, southern Brazil. *Zootaxa*, *3764*, 240–278.

Sarigül, V. (2016). New basal dinosauromorph records from the Dockum Group of Texas, USA. *Palaeontologia Electronica*, *19*, 1–13.

Sarigül, V. (2017). New theropod fossils from the Upper Triassic Dockum Group of Texas, USA, and a Brief Overview of the Dockum Theropod Diversity. *PaleoBios*, *34*, 1–18.

Sarigül, V. (2018). New archosauromorph fragments from the Dockum Group of Texas and assessment of the earliest dinosaurs in North America. *Historical Biology*, *30*, 1059–1075.

Sawin, H. J. (1947). The pseudosuchian reptile *Typothorax meadei*. *Journal of Paleontology*, *21*, 201–238.

Scheyer, T. M., Desojo, J. B., & Cerda, I. A. (2014). Bone histology of phytosaur, aetosaur, and other archosauriform osteoderms (Eureptilia, Archosauromorpha). *The Anatomical Record*, *297*, 240–260.

Schoch, R. R. (2007). Osteology of the small archosaur *Aetosaurus* from the Upper Triassic of Germany. *Neues Jahrbuch für Geologie und Paläontologie Abhandlungen*, *246*, 1–35.

Schoch, R. R., & Desojo, J. B. (2016). Cranial anatomy of the aetosaur *Paratypothorax andressorum*. *Neues Jahrbuch für Geologie und Paläontologie Abhandlungen*, *279*, 73–95.

Seidel, M. R. (1979). The osteoderms of the American *alligator* and their functional significance. *Herpetologica*, *35*, 375–380.

Small, B. (2002). Cranial anatomy of *Desmatosuchus haplocerus* (Reptilia: Archosauria: Stagonolepididae). *Zoological Journal of the Linnean Society*, *136*, 97–111.

Small, B., & Martz, J. W. (2013). A new aetosaur from the Upper Triassic Chinle formation of the Eagle Basin, Colorado, USA. In S. J. Nesbitt, J. B. Desojo, & R. B. Irmis (Eds.), *Anatomy, phylogeny, and Palaeobiology of early archosaurs and their kin: Geological society* (Vol. 379, pp. 393–412). Special Publications.

Small, B. J. (1997). A new procolophonid from the Upper Triassic of Texas, with a description of tooth replacement and implantation. *Journal of Vertebrate Paleontology*, *17*, 674–678.

Spielman, J. A., & Lucas, S. G. (2012). Tetrapod fauna of the Upper Triassic Redonda formation, east-Central New Mexico. *New Mexico Museum of Natural History and Science Bulletin*, *55*, 1–119.

Spielmann, J. A., Hunt, A. P., Lucas, S. G., & Heckert, A. B. (2006). Revision of *Redondasuchus* (Archosauria: Aetosauria) from the Upper Triassic Redonda formation, New Mexico, with a description of a new species. In J. D. Harris, S. G. Lucas, J. A.

Spielmann, M. G. Lockley, A. R. C. Milner, & J. I. Kirkland (Eds.), *The Triassic-Jurassic terrestrial transition* (Vol. 37, pp. 583–587). New Mexico Museum of Natural History and Science Bulletin.

Stocker, M. R., & Butler, R. J. (2013). Phytosauria. In S. J. Nesbitt, J. B. Desojo, & R. B. Irmis (Eds.), *Anatomy, phylogeny, and Palaeobiology of early archosaurs and their kin: Geological society* (Vol. 379, pp. 91–117). Special Publications.

Taborda, J. R. A., Heckert, A. B., & Desojo, J. B. (2015). Intraspecific variation in *Aetosauroides* Casamiquela (Archosauria: Aetosauria) from the Upper Triassic of Argentina and Brazil: An example of sexual dimorphism? *Ameghiniana*, *52*, 173–187.

Teschner, E. M., Konietzko-Meir, D., Desojo, J. B., Schoch, R. R., & Klein, N. (2023). Triassic nursery? Evidence of gregarious behavior in juvenile pseudosuchian archosaurs as inferred by humeral histology of *Aetosaurus ferratus* (Norian; southern Germany). *Journal of Vertebrate Paleontology*, *42*, e2168196.

von Baczko, M. B., Desojo, J. B., Gower, D. J., Ridgely, R., Bona, P., & Witmer, L. M. (2021). New digital braincase endocasts of two species of *Desmatosuchus* and neurocranial diversity within Aetosauria (Archosauria: Pseudosuchia). *The Anatomical Record*, *305*, 2415–2434.

von Baczko, M. B., Taborda, J. R. A., & Desojo, J. B. (2018). Paleoneuroanatomy of the aetosaur *Neoaetosauroides engaeus* (Archosauria: Pseudosuchia) and its paleobiological implications among archosauriformes. *PeerJ*, *6*, e5456.

Walker, A. D. (1961). Triassic reptiles from the Elgin area: *Stagonolepis*, *Dasygnathus* and their allies. *Philosophical Transactions of the Royal Society B*, *244*, 103–204.

Walker, S., & Holbrook, J. (2023). Structures, architecture, vertical profiles, palaeohydrology, and taphonomy of an upper-flow-regime-dominated fluvial system, the Triassic Dockum Group of Palo Duro Canyon, Texas. *Sedimentology*, *70*, 645–684.

Zeigler, K. E., Heckert, A. B., & Lucas, S. G. (2003). A new species of *Desmatosuchus* (Archosauria: Aetosauria) from the Upper Triassic of the Chama Basin, north-Central New Mexico. *New Mexico Museum of Natural History and Science Bulletin*, *21*, 215–219.

Zittel, K. A. (1887–1890). Handbuch der Palaeontologie. 1. Abteilung: Palaeozoologie, 3. Oldenbourg, München and Leipzig, pp. 899.

SUPPORTING INFORMATION

Additional supporting information can be found online in the Supporting Information section at the end of this article.

How to cite this article: Reyes, W. A., Martz, J. W., & Small, B. J. (2024). *Garzapelta muelleri* gen. et sp. nov., a new aetosaur (Archosauria: Pseudosuchia) from the Late Triassic (middle Norian) middle Cooper Canyon Formation, Dockum Group, Texas, USA, and its implications on our understanding of the morphological disparity of the aetosaurian dorsal carapace. *The Anatomical Record*, e25379. https://doi.org/10.1002/ar.25379